

Extragalactic HI Surveys

Riccardo Giovanelli · Martha P. Haynes

Received: date / Accepted: date

Abstract We review the results of HI line surveys of extragalactic sources in the local Universe. In the last two decades major efforts have been made in establishing on firm statistical grounds the properties of the HI source population, the two most prominent being the HI Parkes All Sky Survey (HIPASS) and the Arecibo Legacy Fast ALFA survey (ALFALFA). We review the choices of technical parameters in the design and optimization of spectro-photometric “blind” HI surveys, which for the first time produced extensive HI-selected data sets. Particular attention is given to the relationship between optical and HI populations, the differences in their clustering properties and the importance of HI-selected samples in contributing to the understanding of apparent conflicts between observation and theory on the abundance of low mass halos. The last section of this paper provides an overview of currently ongoing and planned surveys which will explore the cosmic evolution of properties of the HI population.

Keywords First keyword · Second keyword · More

1 Introduction

A number of important HI line surveys have been carried out in the last decade, bringing new insights in particular to the properties of the extragalactic population at $z \simeq 0$. Those surveys have been made possible by the advent of focal plane receiver arrays and telescope upgrades, which have increased the survey speeds by an order

R. Giovanelli
302 Space Science Building, Cornell University, Ithaca NY 14853 USA
Tel.: +001-607-2556505
E-mail: riccardo@astro.cornell.edu

M.P. Haynes
530 Space Science Building, Cornell University, Ithaca NY 14853 USA
Tel.: +001-607-2550610
E-mail: haynes@astro.cornell.edu

of magnitude with respect to what was possible before their inception. While large surveys of HI in galaxies had been carried out in the 1980s and 1990s, those were targeted on optically selected samples generally motivated by goals other than the understanding of the characteristics of the HI source population. For example, large samples of disk galaxies have been observed to map the large-scale structures in the local Universe, or to measure the cosmological peculiar velocity field, or study the environment in clusters, but in those studies HI sources were tools, the support riders in the *peloton*, rather than the cycling team leader. We learned much about the properties that made an HI source a good cosmic lamp post, but we did not know the shape of the cosmic HI mass function. The first “blind” HI surveys, such as AHSS and ADBS, started bringing to our attention the characteristics of the dwarf galaxy population, and the following larger surveys confirmed the fact that the most abundant “island universes” are in fact low mass systems barely able to hold on to a fraction of their baryons and, even more extreme, far less able to convert those baryons into stars. Some toyed with the idea that these systems would be so abundant that they would fill the gap between the counts of low mass galaxies and that of low mass halos predicted by theory, known and not satisfactorily explained since the onset of the Λ CDM paradigm. The now solid determination of the HI mass function demonstrates that idea to be wrong. However, the new surveys are suggesting interesting avenues that may lead to a solution of the “problem”, so we devote a fair fraction of this review to the investigation of these developments.

We start Section 2 by visiting a set of scaling relations, useful in the planning and design of a survey. We close that section with an illustration of the power of a blind survey data set in reaching very deep in signal extraction, by careful application of stacking techniques. In Section 3 we review the properties of the HI source population, from the clustering characteristics to the HI mass function, the relationships between gas content and properties in spectral domains other than HI, to the HI view of star formation laws, closing with the baryonic mass function and the assessment of the baryon deficit of small mass halos. Section 4 is a show-and-tell interlude, in which we describe the extreme properties of a few sources in the ALFALFA catalog. Section 5 explores the conflicts between observations and Λ CDM predictions arising from the use of the abundance matching technique. The last section is dedicated to a highlights report of proposed (and some already started) new surveys. Sky positions are for the epoch 2000.0 and distances are derived for $H_0 = 70 \text{ km s}^{-1} \text{ Mpc}^{-1}$, unless otherwise specified.

2 Review and Status of Large HI Surveys

2.1 Survey Design Tools

The sensitivity of a radio telescope depends primarily on (a) the system’s “gain” G , which to first order is the area of its primary mirror; (b) the noise contributed by the electronics, ground, atmospheric and cosmic sources of radiation, which is measured by the system temperature T_{sys} ; and (c) the frequency bandwidth $\Delta \nu$ over

which radiation is collected. This is summarized by the radiometer equation

$$\sigma_{rms} = (T_{sys}/G)(2 \Delta v t_{int} f_x)^{-1/2} \quad (1)$$

where σ_{rms} is the rms noise of a spectrum with the telescope pointing at blank sky, t_{int} is the integration time, f_x , of order unity, accounts for source angular extent, observational switching technique, bandpass subtraction mode, spectrometer clipping losses, etc., and the factor of 2 accounts for the addition of two independent polarization channels. In the computation of sensitivity, Δv will refer to the spectral resolution needed to detect and resolve the narrowest signal the survey will be sensitive to; in the estimate of survey speed, Δv will be the instantaneous bandpass of the receiver system. Most of the HI in a galaxy is found in a warm, neutral, optically thin thermal phase of several 10^3 K and the solid angle subtended by the cold neutral phase of the interstellar medium is small, so the mass of a spatially unresolved, optically thin source at the luminosity distance D_{Mpc} , expressed in Mpc, is

$$\frac{M_{HI}}{M_\odot} = \frac{2.356 \times 10^5 D_{Mpc}^2}{1+z} \int S(V) dV, \quad (2)$$

where $S(V)$ is the line profile in Jy, integrated over the Doppler velocity V in km s^{-1} . Approximating $\int S(V) dV \simeq S_{peak} W_{50}$, the product of peak flux times the line width at the 50% level, the signal-to-noise ratio (S_{peak}/σ_{rms}) can be used to infer the scaling of the minimum detectable HI mass at the distance D_{Mpc}

$$M_{HI} \propto (T_{sys}/G) D_{Mpc}^2 W_{50}^{-\gamma} t_{int}^{-1/2} \quad (3)$$

Figure 1 shows the flux distribution of sources detected by ALFALFA, as a function of their line widths. The exponent γ is -1 for $W_{50} < 200 \text{ km s}^{-1}$, and it changes progressively to $\gamma \simeq -2$ for $W_{50} > 200 \text{ km s}^{-1}$, due to the impact of standing waves on the spectral baselines.

A blind, spectro-photometric HI survey does not deliver a flux-limited source sample, but rather one in which the sensitivity limit is a function of the spectral linewidth of the source. In the case of the ALFALFA survey, with an average integration time $t_{int} \simeq 48$ seconds per beam solid angle, an HI source with $W_{50} = 25 \text{ km s}^{-1}$ and $M_{HI} = 10^6 M_\odot$ can be detected to a distance of 6.5 Mpc, and a source of HI mass $10^7 M_\odot$ to a distance of 20 Mpc, as illustrated in Figure 2.

A useful scaling relation regards the minimum integration time required to detect a source of HI mass M_{HI} , line width $W_{50} \text{ km s}^{-1}$, at the distance D_{Mpc}

$$t_{int} \propto (T_{sys}/G)^2 M_{HI}^{-2} D_{Mpc}^4 W_{50}^{-2\gamma} \quad (4)$$

i.e. the depth of a survey of given T_{sys}/G increases only as $t_{int}^{1/4}$. For a given HI mass, the volume sampled by a survey with a telescope of given T_{sys}/G is

$$V_{survey}(M_{HI}) = \Omega_{survey} D_{max}^3 / 3 \propto \Omega_{survey} t_{int}^{3/4} \quad (5)$$

where Ω_{survey} is the solid angle covered by the survey and D_{max} is the maximum distance at which the mass M_{HI} can be detected. That volume is proportional to the

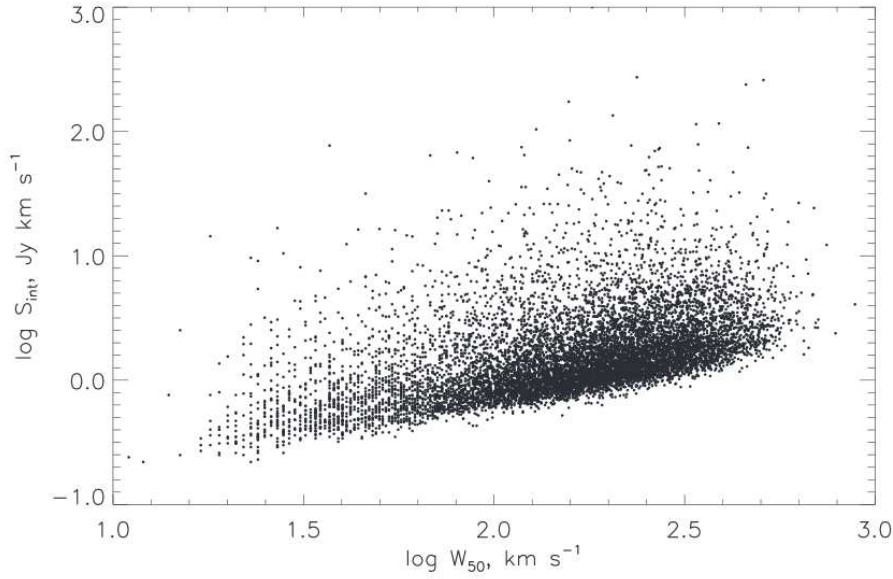


Fig. 1 Log of the HI flux vs. velocity width of HI sources detected by ALFALFA. γ refers to the slope of the lower boundary of the data points, which steepens for $W_{50} > 200 \text{ km s}^{-1}$.

number of sources detected by the survey, so the time necessary to complete it is $t_{\text{survey}} \propto (\Omega_{\text{survey}}/\Omega_b)t_{\text{int}}$, where Ω_b is the telescope beam (or beams, for arrays), thus

$$t_{\text{survey}} \propto V_{\text{survey}} t_{\text{int}}^{1/4} \quad (6)$$

i.e. for a fixed Ω_{survey} , the time required to complete it increases as $t_{\text{int}}^{1/4}$. Once t_{int} is large enough for a desired M_{HI} to be detectable, it is more advantageous to maximize Ω_{survey} than to increase the survey depth by increasing t_{int} . For example, in the design of the ALFALFA survey it was desired that the survey sample median distance correspond to a fair cosmological distance of $\simeq 100 \text{ Mpc}$, the choice of which determined t_{int} . After that, the survey volume was obtained by expanding Ω_{survey} .

In the case of blind surveys carried out with a single dish, such as HIPASS and ALFALFA, the vast majority of detected sources have angular size much smaller than the telescope beam. The photometric parameter used for their characterization is then the line flux integral, information on the morphology and spatial extent of the source being lost. A lower limit for the averaged HI column density of the source can be obtained, by dividing the HI mass by the areal extent subtended by the beam. For a telescope with an elliptical beam, such as the case of the Arecibo antenna with its 7-horn feed array ("ALFA"), with major and minor axes θ_1 and θ_2 (FWHP, in arcminutes):

$$\bar{N}_{\text{HI}} = \frac{2.34 \times 10^{20}}{\theta_1 \theta_2} (1+z)^4 \int s(v) dv \quad (\text{cm}^{-2}) \quad (7)$$

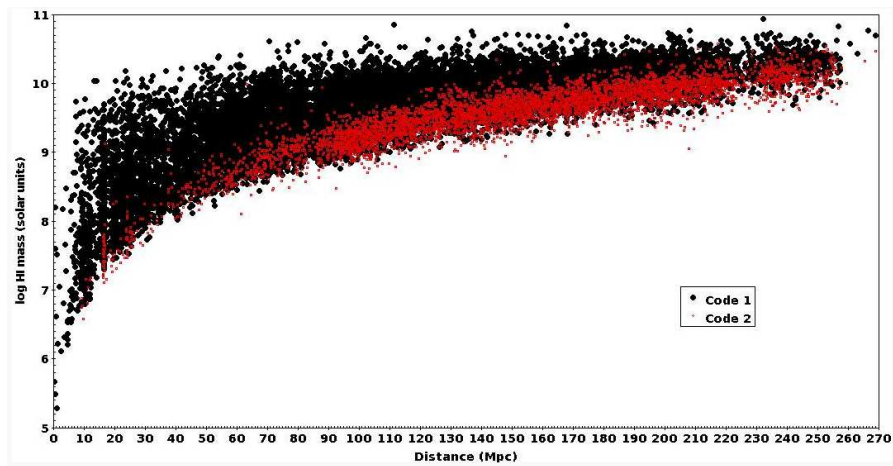


Fig. 2 Log of the HI mass distribution vs. distance of HI sources detected by ALFALFA. Black symbols identify sources of high signal-to-noise - greater than 6.5 -, while red symbols refer to sources of signal-to-noise between 4.5 and 6.5, corroborated by having an a priori known redshift which matches the ALFALFA detection. A gap in the data near $D_{Mpc} \simeq 230$ is produced by radio frequency interference (RFI) originating in the San Juan airport radar; a lesser dip near $D_{Mpc} \simeq 85$ is due to transmissions associated with the Global Positioning System (GPS), as we discuss in Section 2.3.

Large single dishes with focal plane detector arrays, such as the Arecibo and Parkes telescopes, are well suited to carry out wide field, blind HI extragalactic surveys, such as ALFALFA and HIPASS. However, follow-up synthesis imaging is necessary in order to obtain direct information on dynamical parameters, such as the mass contained within the HI radius of the source and the shape of the rotation curve. Synthesis imaging can provide maps of HI column densities, but can wholly miss flux from diffuse regions extending over solid angles exceeding that of the synthesized beam. A combination of both types of instrument is thus the most economical and scientifically rewarding: the single dish survey is most efficient in delivering large samples, characterizing the statistical properties of the HI source population, and discovering the most extreme member of such population; the synthesis arrays allow the investigation of the structure, dynamics and physical circumstances of selected sources.

2.2 Types of Surveys

Before the 1990s, large extragalactic HI surveys were carried out, seeking detection of optically selected galaxy samples. For these surveys, the task of understanding the properties of the HI source population was secondary to that of using the HI source samples as tools towards the achievement of other scientific goals, such as the impact of environment on gas bearing objects in clusters, the determination of the parameters of the cosmological distance scale, the investigation of the topology of the large scale distribution of galaxies and mapping the deviations from smooth Hubble flow produced by large scale density inhomogeneities. The studies with the largest

numbers N_{det} of detections were obtained with the Arecibo ($N_{det} \sim 10^4$), Nançay, Parkes and Green Bank (a few 10^3 each) telescopes. The most conspicuous bias in the selection of sample candidates for these studies was a preference for high optical luminosity systems, morphologically classified as disks, which tended to neglect field dwarfs. An interesting statistic illustrating this bias is that more than 2/3 of detections by ALFALFA correspond to galaxies never observed before in the HI line. Results of these studies are documented in reviews and data releases such as Haynes et al. (1984), Aaronson et al. (1982), Fisher & Tully (1981), Giovanelli & Haynes (1991), Roberts & Haynes (1994), Bottinelli et al. (1990), Haynes et al. (1999), Mathewson & Ford (1996). These surveys will not be reviewed further.

The first strictly blind and moderately blind extragalactic HI surveys were made at Arecibo in the late 1990's, during the period in which the telescope was being upgraded. Two surveys (AHISS: Zwaan et al. 1997; ADBS: Rosenberg & Schneider 2000) provided the first indications of the statistical importance of the field dwarf galaxies, whose baryonic component is dominated by atomic gas rather than stars. HIPASS (Meyer et al. 2004) was the first truly wide-field, extragalactic HI survey, covering 3/4 of the whole sky with its 13-element focal plane detector array.

With its large collecting aperture, the 53 year old 305m telescope at Arecibo remains the most sensitive HI detector. During its first 30 years of operation, its use as a blind survey machine was limited due to the fact that the correction of the spherical aberration of its primary mirror was achieved by means of line feeds. These are waveguide contraptions with very narrow instantaneous bandwidth and lacking a usable, extended field of view, which constrained to single pixel observations. Completion of the Gregorian Upgrade in the late 1990s expanded the field of view, making possible the installation of receiver arrays, broadening the bandwidth to 300 MHz; sensitivity was further increased by improving the illuminated area of the primary mirror and installing a 1-km long screen, peripheral to the primary, that reduced ground radiation pick-up and improved performance at high zenith angles. Operating in L-band, the 7-beam ALFA (Arecibo L-band Feed Array) array became available in 2005. Several HI surveys with ambitious goals were then started. Of particular interest were the four extragalactic HI surveys: Arecibo Legacy Fast ALFA (ALFALFA, Giovanelli et al. 2005), Arecibo Galactic Environment Survey (AGES, Auld et al. 2006), ALFA Zone of Avoidance Deep Survey (ZOA, Henning et al. 2008) and Arecibo Ultra Deep Survey (AUDS, Freudling et al. 2011).

A comparison of major blind surveys of the last two decades is shown in Table 1, which illustrates angular resolution, survey solid angle, spectral resolution, noise figure, median redshift and number of detections, respectively from columns 2 to 7. The noise figure is expressed for a common value of spectral resolution of 18 km s^{-1} , although several surveys have observed with much higher spectral resolution. The AUDS and ZOA surveys have reported on preliminary results (Henning et al. 2010; McIntyre et al. 2015; Hoppmann et al. 2015) and have plans for more extensive work. The AGES team is accumulating data over a number of specially targeted regions spanning a range of environments, from isolated systems to the Virgo and A1367 clusters. Preliminary AGES results (Davies et al. 2011) suggest a steeper mass function ($\alpha \sim 1.52 \pm 0.05$) than those reported by either HIPASS or ALFALFA, though this result is currently based only on 370 galaxies.

Table 1 Comparison of Major Blind HI Surveys

Survey	Beam '	Area deg ²	δ_v km s ⁻¹	rms ^d mJy	V_{med} km s ⁻¹	N_{det}	Ref
AHISS	3.3	13	16	0.7	4800	65	^b
ADBS	3.3	430	34	3.3	3300	265	^c
HIPASS	15.	30000	18	13	2800	5000	^{d,e}
AGES	3.5	200	11	0.7	9500	2900	^f
ALFALFA	3.5	6920	11	1.7	8200	31000	^g
AUDS	3.5	2.7	5	0.08	22000	200	^h
ZOA	3.5	300	5	0.7	6500	1200	ⁱ

^a mJy per beam at 18 km s⁻¹ resolution; ^b Zwaan et al. (1997); ^c Rosenberg & Schneider (2000); ^d Meyer et al. (2004); ^e Wong et al. (2006); ^f projection, based on results of 30% data release: www.naic.edu/ages/public; ^g Giovanelli et al. (2005) and projection for high signal-to-noise objects only, based on results of 70% catalog; ^h based on detection of 102 sources in half of the projected survey coverage (Hoppmann et al. 2015); ⁱ based on detection of 61 sources over 15 sq. deg. section out of 300 sq. deg. projected coverage (McIntyre et al. (2015)).

After the pilot surveys AHISS and ADBS, HIPASS was completed with great success. It covers 3/4 of the whole sky, detecting about 5000 sources at a median redshift $cz \simeq 2800$ km s⁻¹, for a sky density of one detection every 6 deg². Two major surveys have been completed with the ALFA feed array at Arecibo: ALFALFA and AGES. The statistics of AGES is difficult to compare with that of other surveys, since that survey is a collection of selected fields of specific interest, such as galaxy cluster fields (e.g. A1367) and the near fields of objects with tidal remnants (e.g. NGC 7332/7339), each field being mapped blindly, but characterized by different environmental properties. The total area mapped by AGES is about 200 deg², for a detection rate of ~ 15 sources per deg², partly resulting from the deep sensitivity limit of 0.7 mJy and partly to the selection of *a priori* known to be significantly overdense regions. ALFALFA covers a solid angle of $\simeq 7000$ deg² with a sensitivity of 1.7 mJy at the 18 km s⁻¹ spectral resolution. The current ALFALFA catalog, which covers 70% of the survey area, contains 27,000 sources, thus the complete catalog will exceed the count of 30,000 sources, for a detection rate of about 4.5 sources per deg², an increase in the HIPASS detection rate per unit area by a factor of ~ 20 . With a source median redshift of $cz \simeq 8000$ km s⁻¹, ALFALFA is the first blind HI survey approaching coverage of a cosmologically fair volume, for sources at its median redshift. ZOA is a survey aimed to inspect connectivity across the galactic plane, of large-scale features in the galaxy distribution. With a nominal sensitivity about 2.5 times better than ALFALFA's, it should yield a significantly larger detection rate per deg² and median velocity. However its detection rate is 4.2 deg⁻² and its median cz is less deep than ALFALFA's. This is in part due to a less efficient bandpass calibration technique, forced by running "piggyback" on a pulsar survey. AUDS is the deepest of the HI surveys to date. It maps two roughly antipodal sky regions for a total solid angle of 2.7 deg². The first data release reports the detection of 102 galaxies over 1110 hours of telescope time, with a sensitivity level σ_{rms} of 80 μ Jy and a median $cz \simeq 22,000$ km s⁻¹. The low efficiency of the detection rate in this case is due to

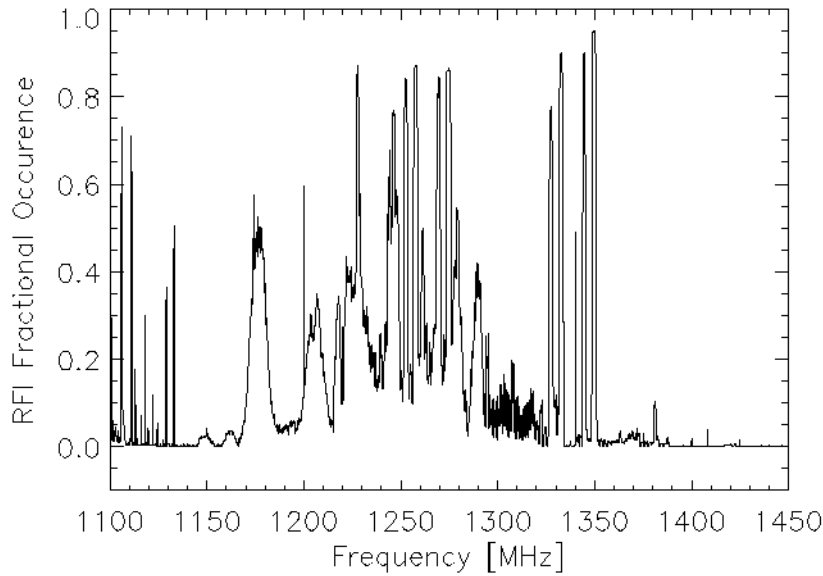


Fig. 3 L-Band RFI at the Arecibo Observatory. The fractional occurrence of RFI, i.e. the fraction of the time that observations are severely affected by RFI at any given frequency at the Arecibo Observatory, sampled with a resolution of 0.1 MHz. The 21cm line rest frequency is 1420.4 MHz. Credit: P. Perillat (2015).

the bad conditions of RFI) at frequencies lower than ~ 1350 MHz ($z > 0.05$), as we discuss in section 2.3.

The low efficiencies of ZOA and AUDS illustrate the impact of circumstances not considered by the scaling relations drawn in this section. On the positive side, it emphasizes the synergies in allowing different surveys sharing simultaneous use of the telescope, as in the cases of ZOA riding piggyback on a pulsar survey and the interstellar HI survey TOGS doing so with ALFALFA. On the negative side the observing mode imposed by the pulsar survey on ZOA may not be optimal for the latter. In the case of AUDS, the noisy spectral environment of Arecibo underscores the importance of site selection for the new generation facilities in Western Australia, China and South Africa.

Other blind surveys of somewhat lesser impact are discussed in Henning et al. (2000), Minchin et al. (2004), Lang et al. (2003), Davies et al. (2004). Prominent targeted surveys with relatively small samples but high parametric content, carried out with HI synthesis arrays, are THINGS (Walter et al. 2008), LittleTHINGS (Hunter et al. 2012), FIGGs (Begum et al. 2008) and SHIELD (Cannon et al. 2011).

2.3 RFI

The worst enemy of a spectro-photometric, extragalactic HI survey is radio frequency interference (RFI), such as airport radar, orbit-to-ground data download, radio stations, cell phone transponders, etc. Alleviating techniques fall short of clearing the impact of more than a small fraction of RFI sources, so that the quality of survey data suffers selectively at different epochs and frequency bands. An example of this impact is shown in Figure 3, which displays the fraction of the time for RFI occurrence, plotted as a function of frequency and averaged over the year preceding August 1st, 2015 at the Arecibo Observatory (Perillat 2015). The radio L-band spectrum is relatively clean for extragalactic HI observations at frequencies higher than ~ 1350 MHz ($z_{HI} < 0.06$), the major disturbance being the Global Positioning System (GPS), emitting near 1381 MHz about 10% of the time. At increasing z for the HI line, the next important RFI source is the San Juan airport radar, transmitting between 1325 and 1350 MHz. Below 1325 MHz a multitude of RFI sources occupy the spectrum. In Fig. 2, the gap in the source density of sources near $D_{Mpc} = 230$ corresponds to the frequency range obliterated by the transmissions of the San Juan airport radar, located about 100 km from the Arecibo telescope. Apart from GPS, the spectral band between 1350 MHz and 1420 MHz is relatively clean at Arecibo, still allowing largely unpolluted observing conditions. However, at 1350 MHz and below RFI is very severe.

2.4 Stacking

An option available with blind HI survey data is that of obtaining estimates of average properties of specific categories of sources, to noise levels significantly lower than those achievable for single sources. Suppose that a population of sources — for example early type galaxies — falls within the volume sampled by a survey, but the survey sensitivity is not sufficient to individually detect more than a small subsample of the lot. If the positions and recession velocities of the sources are known, co-adding the survey spectra along the line of sight of a number N — which can be large — of individually undetected sources can reduce the noise and deliver a significantly deeper sensitivity measure of the statistics of the population. Before co-adding, each spectrum needs to be shifted in frequency by an amount which aligns its recession velocity with that of the other spectra to be stacked. For the ALFALFA survey, the rms noise of the co-added spectrum can be seen to decrease nearly as $N^{-1/2}$, as shown in Fig. 4 (Fabello et al. 2011).

Figure 5 illustrates the power of the stacking technique, as applied to the study of HI content in early type galaxies (ETG) by Fabello et al. (2011). An optically selected parent sample of 4748 ETGs was extracted from the Sloan Digital Sky Survey, a subset of only $\simeq 20\%$ of which had been individually detected by ALFALFA. The parent sample was subdivided into 5 bins of stellar mass (only the top 3 are shown in the figure), and the ALFALFA spectra at the location of each galaxy in the mass bin were co-added. Panels in the left column show the result of the co-addition of all galaxies within the bin, including galaxies individually detected by ALFALFA;

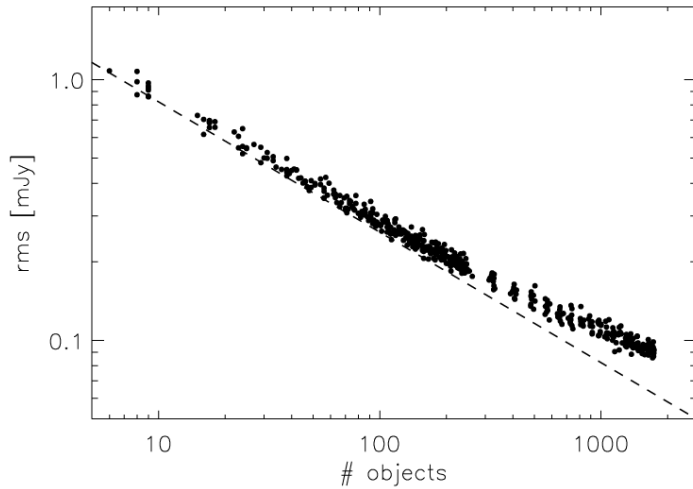


Fig. 4 Noise figure of stacked spectra, as a function of the number of objects co-added. The dashed line is the expected $N^{-1/2}$ dependence for clear non-Gaussian noise, after Fabello et al. (2011).

panels in the column to the right show the result from co-adding only spectra with no individual evidence of emission. E.g. for the top mass bin, which includes 1734 galaxies with stellar mass between $10^{10.0}$ and $10^{10.3} M_{\odot}$, 1417 show no evidence of individual emission. However, the co-addition of the 1417 objects shows a clear detection with a signal-to-noise ratio of ~ 50 . As indicated in Section 2.1, ALFALFA can detect an HI mass of $\sim 10^7 M_{\odot}$ at a distance of 20 Mpc. Figure 4 shows that the technique can reduce σ_{rms} by a factor of ~ 20 ; the HI mass detection limit scales linearly with σ_{rms} , so ALFALFA can set a limit of $\sim 5 \times 10^5 M_{\odot}$ for stacked sources located at 20 Mpc.

The impact of confusion on stacking is discussed, eg. by Delhaize et al. (2013), Duffy et al. (2008) and Jones et al. (2015b). The signal fraction derived from the accumulated emission of targeted, central sources is mixed with a confusion signal accumulated along the line of sight. The latter is referred to as the “confused mass”. Fabello et al (2011) find that a factor of 10-20 below the detection limit is the most that could be gained by stacking, before non-Gaussian noise becomes dominant, as shown by Fig. 4. The confused mass grows rapidly with redshift of the survey, dominating stacked spectra for $z > 0.1$ in surveys carried out with single dishes.

3 Properties of the HI Source Population

The fundamental properties of individual galaxies correlate strongly: massive galaxies are brighter and larger than less massive ones, but they also tend to be redder, of higher metallicity and dustier. At its simplest, the Hubble sequence illustrates how strongly galaxy morphology correlates with metrics associated with color which in turn reflect the history of star formation. The huge digital dataset produced by the Sloan Digital Sky Survey has enabled the robust determination of uniformly mea-

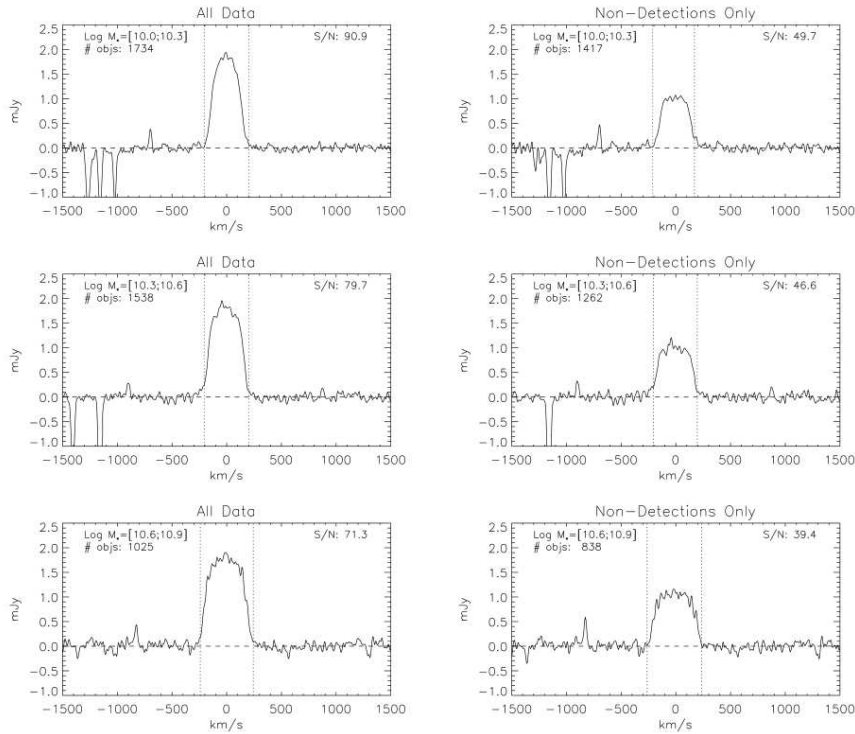


Fig. 5 Co-added spectra of an optically selected sample of early type galaxies are shown, for three stellar mass bins. ALFALFA detects only about 1/5 of the objects. For each of the mass bins, panels to the left show the co-added line profile of all galaxies within that bin, including those individually detected; panels to the right show the line profile obtained by co-adding only the spectra of non-detections. The inset labels within each box are (i) the stellar mass range over which spectra have been stacked; (ii) the number of co-added spectra and (iii) the Signal-to-noise ratio of the co-added spectrum. The narrow features near $cz \simeq -1000$ km s $^{-1}$ and below are due to rfi. Credit: Fabello et al. (2011).

sured properties to place on a quantitative basis the interrelationships among stellar mass, optical luminosity, mass-to-light ratio, star formation rate, mean stellar age, size, metallicity, velocity dispersion and rotational velocity for the $z = 0$ Universe. These observational relations for the local galaxies serve as the end-point for models of the evolution of galaxies over cosmic time, giving rise to the “galaxy main sequence”, i.e. the tight correlation at any given redshift between a galaxy’s star formation rate and its stellar mass. Most of these studies focus on massive galaxies with $\log M_{star} > 10.5$ the majority of which lie on the “red-sequence” and are no longer forming stars.

In contrast to the wide area optical/IR surveys, the HI surveys sample a very different population of galaxies, largely excluding the red and dead galaxies. Not all galaxies contain (detectable) HI and it is important to understand the resultant bias on the HI source population. After reviewing the clustering properties of the HI source population and its distribution as a function of HI mass, in this section we discuss

our fundamental understanding of the HI-selected population with emphasis on how it strongly differs from an optically selected one.

3.1 The HI Auto-correlation Function

The morphology-density relation which describes the clustering properties of galaxies is more often statistically quantified by the measurement of correlation functions. In its simplest form, the autocorrelation function in real space $\xi(r)$ counts pairs of objects as a function of their separation vector, which is derived from a component r_p in the plane of the sky and one along the line of sight π . Redshift space distortions acting on different scales need correcting in order to yield a reliable $\xi(r)$. A power law function is fitted, $\xi(r) = (r/r_o)^{-\gamma}$. Guzzo et al. (1997) estimated the power law parameters as a function of morphological type: $r_o = 8.35 \pm 0.75 h^{-1}$ Mpc and $\gamma = 2.05 \pm 0.09$ for ellipticals and $r_o = 5.55 \pm 0.45 h^{-1}$ Mpc and $\gamma = 1.73 \pm 0.08$ for Sb and earlier spirals; for later spirals and irregulars, they obtained $r_o = 4.05 \pm 0.70 h^{-1}$ Mpc and $\gamma = 1.5 \pm 0.12$. Defining the relative bias parameter b between elliptical and early spiral populations as $\xi_E(r) = b^2 \xi_S(r)$, they get $b = 2.0 \pm 0.4$ with only a very mild dependence on scale r . The spiral population is antibiased with respect to the elliptical one.

The optical counterparts of HI-rich galaxies are very frequently blue, low optical surface brightness systems, which are known to favor low density environments. Thus, it is not surprising that HI-selected samples exhibit similar clustering properties. With important SKA precursor experiments being built with the goal of characterizing the HI source populations at intermediate redshifts, it is important to establish soundly the statistical properties of those objects at $z = 0$. The HIPASS and ALFALFA surveys have recently been used for the derivation of the autocorrelation function of the HI source population. Meyer et al. (2007) and Basilakos et al. (2007) both agreed in identifying the HIPASS HI sample as the extragalactic population with the weakest clustering known; the two groups found respectively best fits of 3.5 ± 0.3 and $3.3 \pm 0.4 h^{-1}$ Mpc for r_o and 1.47 ± 0.08 and 1.4 ± 0.2 for γ . While Basilakos et al. (2007) found that, within the HI population, high mass sources clustered more strongly, Meyer et al. (2007) found no statistical difference between high and low mass subsamples. Using the ALFALFA $\alpha.40$ catalog, Martin et al. (2012) found $r_o = 3.3 \pm 0.3 h^{-1}$ Mpc and $\gamma = 1.51 \pm 0.09$, a very good match with the results based on the HIPASS data. The HI selected population is thus antibiased with respect to all optical samples.

It is convenient to compare the autocorrelation function of the $\alpha.40$ catalog with that of the dark matter halos as produced by Λ CDM simulations. Then, the bias parameter is shown by Martin et al. (2012) as a function of scale in the left hand panel of figure 6. The HI galaxy population is antibiased with respect to that of the dark matter. The left hand panel of figure 6 shows the autocorrelation of the ALFALFA $\alpha.40$ catalog and its best fit model (dashed line). The solid line is the real-space autocorrelation function of the dark matter halos $\xi_{DM}(r)$. The right hand panel of figure 6 shows the bias parameter as a function of scale. Dark matter is clearly more clustered than the HI source population, but the bias is scale dependent. HI selected

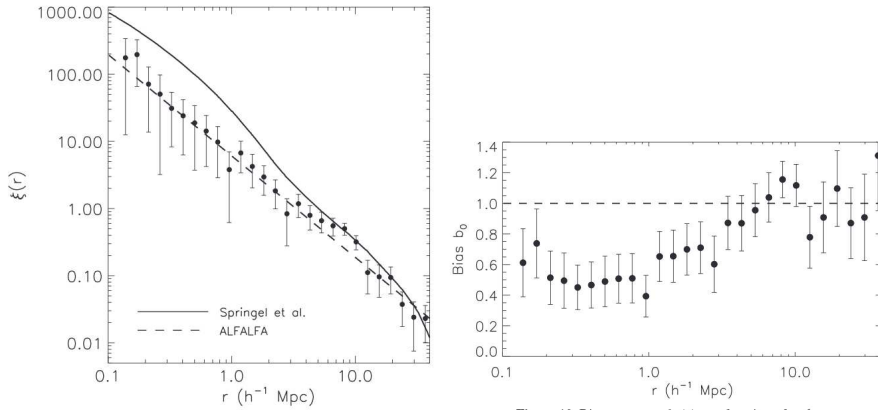


Fig. 6 **Left** Real space autocorrelation function for the dark matter halos from the Millennium simulation (solid line) and for the HI $\alpha.40$ ALFALFA sample (symbols with error bars). **Right:** Bias parameter plotted as a function of scale. Both Figures from Martin et al. (2012)

galaxy samples appear to be severely antibiased on small scales, but only weakly antibiased on large scales.

3.2 The HI Mass Function

The distribution of low mass dark matter halos in Λ CDM simulations can be fit by a Schechter function of slope $\alpha = -1.8$. However, the best fit slope to the faint end of the optical luminosity (or the stellar mass) function of galaxies exhibits a shallower behavior, with slopes typically between -1.0 and -1.3 . Likewise, the early determinations of fits to the HI mass function (HIMF) returned low mass slopes which appeared shallower than that of dark matter halos, both in the case of optically selected samples (Springob et al. 2005) and in that of samples derived from blind surveys (Rosenberg & Schneider 2000). Using the HIPASS source catalog of 4315 HI sources, Zwaan et al. (2003, 2005) obtained $\alpha = -1.37$. However, the HIPASS catalog contained only 44 objects less massive than $10^8 M_{\odot}$, making the determination of the slope uncertain. The ALFALFA catalog $\alpha.40$ contained 10452 high signal-to-noise detections, of which 329 are less massive than $10^8 M_{\odot}$. Moreover, with a median redshift of $cz \simeq 8000 \text{ km s}^{-1}$, vs. the $\simeq 2800$ of HIPASS, ALFALFA samples a cosmologically fair volume which is significantly deeper than that of HIPASS. The ALFALFA HIMF had a best-fit Schechter function of $\alpha = -1.33 \pm 0.02$, very close to the value of Zwaan et al. (2005), a characteristic “knee” mass $M^* = 10^{9.96 \pm 0.02} M_{\odot}$ and a normalization parameter $\phi^* = 4.8 \pm 0.03 \times 10^{-3} \text{ Mpc}^{-3} \text{ dex}^{-1}$. The early mismatch between Λ CDM and actual galaxy counts is now reliably confirmed: there is no detected population of galaxies making the baryonic (stellar plus gas) mass function approach the abundance of low mass dark matter halos.

The HIPASS and $\alpha.40$ HIMFs however disagree in the counts of sources with the highest masses: at $\log M_{\text{HI}}/M_{\odot} = 10.75$ ALFALFA finds $5 \times$ more objects than HIPASS and at $M_{\text{HI}} \simeq 10^{11} M_{\odot}$ the gap widens to one order of magnitude. The

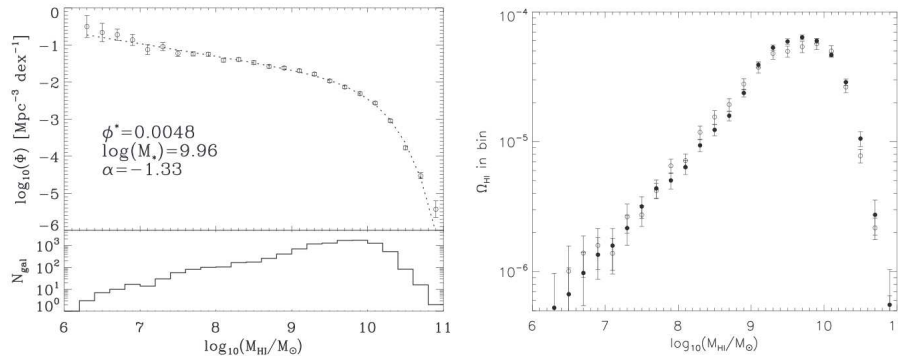


Fig. 7 Upper left: The ALFALFA HIMF, based on the $\alpha.40$ catalog, as obtained via the SWML method, after Martin et al. (2012). Inset are the best fit parameters of a Schechter model. The lower plot is a histogram of the number of HI sources, per mass bin, on a logarithmic scale. **Right hand:** Histogram of the contribution to Ω_{HI} of galaxies binned by HI mass. Filled symbols refer to calculations of the HIMF via the $1/V_{max}$ method, while unfilled ones refer to using the SWML method. The overall density of HI in the $z = 0$ Universe is mainly contributed by galaxies with $9.0 < \log(M_{HI}/M_{\odot}) < 10.0$. Figure after Martin et al. (2012).

$\alpha.40$ HIMF obtained via the stepwise maximum likelihood (SWML, Efstathiou et al. 1988) method is shown in figure 7. Li et al. (2012) have derived a photometric estimator of the HI mass fraction M_{HI}/M_* using the ALFALFA catalog and applied it to a larger sample of 24000 SDSS galaxies in the redshift range $0.025 < z < 0.05$ and found that the bias parameter is a function of both scale, as found by Martin et al. (2012, cf. Figure 6), and HI mass fraction, galaxies with higher mass fraction being significantly more unbiased.

The resulting cosmic density of HI in the $z = 0$ Universe is, according to ALFALFA, a fraction $\Omega_{HI} = (4.3 \pm 0.3) \times 10^{-4}$ of the critical density. While the HI-rich dwarf galaxy population dominates the cosmic density by number, the total density of HI at $z = 0$ is largely contributed by galaxies with $9.0 < \log(M_{HI}/M_{\odot}) < 10.0$, as shown in the right hand panel of Figure 7. In a paper presenting the result of half of their survey (AUDS) data, Hoppmann et al. (2015) report the detection of 102 galaxies with redshifts up to $z = 0.16$ (median $z = 0.065$). This sample yields an HI mass function statistically compatible with those obtained by HIPASS and ALFALFA. By splitting the data into subsets of high and low redshift, they suggest a possible decrease in $|\Omega_{HI}|$ towards the upper end of the redshift range. Combining their results with those of other surveys, they estimate $\Omega_{HI} = (2.63 \pm 0.10) \times 10^{-4}$.

3.3 What galaxies emit HI?

In combination with the large, deep, homogeneous SDSS database, the major HI surveys allow determination of how the HI content and gas fraction vary with comparable properties that describe the stellar component. Figure 8, from Huang et al. (2012b), shows the scaling relations between the HI mass and HI fraction (M_{HI}/M_*) with the stellar mass and (NUV-r) color for the $\alpha.40$ catalog. Contours denote the

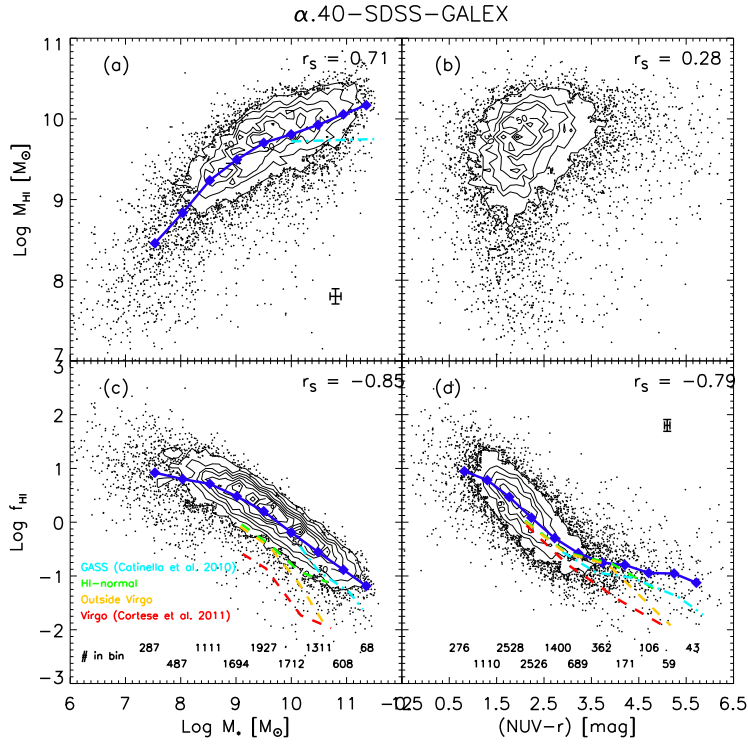


Fig. 8 Scaling relations for the HI mass and atomic gas fraction $f_{HI} = M_{HI}/M_*$ as functions of stellar mass M_* and (NUV-r) color. Contours trace the distribution of galaxies commonly detected by ALFALFA-SDSS-GALEX, with the lowest contour at a level of 20 galaxies per grid cell, contour steps of 20 counts per cell; at lower densities, individual points are plotted. Lines in several panels trace mean relations from the GASS survey Catinella et al. (2010) and the local survey of Cortese et al. (2011). From Huang et al. (2012b).

densely populated regions (cells with 20 or more galaxies), below which individual points are plotted.

Huang et al. (2012) find that a transition in the star formation (SF) properties appears to occur around stellar masses of $M_* \sim 10^{9.5} M_\odot$. Below that break point, the slope of the star-forming sequence changes and the dispersion in the specific star formation rate (SSFR) increases; in fact, at low masses, the SF appears to be strongly regulated by the atomic gas, and the star formation history is bursty and non-continuous. Over the same volume, the population detected by HI surveys has higher overall SFRs and SSFRs at fixed stellar mass. The evidence suggest that the HI-rich galaxies are less evolved than an optically-selected population, either because there is some bottleneck in the conversion of atomic to molecular gas or that the overall star formation law in HI-dominated galaxies is different and relatively inefficient. Curiously, Huang et al. (2012) find that, at a fixed stellar mass, galaxies with higher gas fractions appear also to be hosted by dark matter halos with higher than average

angular momentum (as measured by the observational equivalent of the spin parameter λ).

3.4 What galaxies don't HI surveys see?

Canonical understanding states that early-type galaxies (ETGs) contain very little cool gas and that disk galaxies in the cores of rich clusters are highly HI-deficient relative to comparable galaxies in the field, notably as a result of ram pressure stripping.

Early type galaxies (ETGs) in general are “red and dead”, assumed having long ago converted their atomic gas supply into stars. Of course, that stereotype is a gross oversimplification with many ETGs, particularly those outside clusters showing modest amounts of HI Grossi et al. (2009). In fact, Serra et al. (2012) summarize the results of HI synthesis mapping, principally with the WSRT, of 166 nearby ETGs also contained in the ATLAS^{3D} survey. The detection rate of this survey is $\sim 10\%$ for ETGs which are Virgo members and $\sim 40\%$ for ETGs outside Virgo. Serra et al. (2014) point out that the HI morphologies of ETGs, as well as their masses, are surprisingly diverse, with about 25% of the field ETGs hosting quite massive (up to $10^9 M_{\odot}$, extended HI disks or rings. Those authors suggest that current simulations do not predict the observed HI properties of ETGs.

3.5 HI-deficient galaxies

That spiral galaxies in clusters are much poorer in their gas content than field dwellers of comparable morphological type and size, and that their gas disks are truncated due to ram pressure stripping, has been known for more than 40 years (Haynes et al. 1983; Giovanelli & Haynes 1983; Boselli & Gavazzi 2006 and refs. therein). More recent studies have investigated the problem in greater detail (Solanes et al. 2002; Vollmer et al. 2004; Chung et al. 2009), bringing more clarity to the understanding of the physical process. The study of HI deficiency is however only marginally aided by blind, shallow surveys like ALFALFA and HIPASS: deep, targeted HI observations are required in order to reliably measure HI deficiency. The one aspect that large, blind surveys can contribute effectively to the measurement of HI deficiency is in the determination of the standard of “HI normalcy”, by measuring the properties of large samples of galaxies found in various stages of isolation (Toribio et al. 2011). In Virgo, the sensitivity of current HI instruments is adequate to probe the lower mass population. Boselli & Gavazzi (2014) review the full body of evidence concerning the formation and evolution of low mass red galaxies in clusters, especially Virgo thanks to its vicinity, confirming the general conclusion that ram pressure stripping of infalling dwarfs is the dominant process, leading to the quenching of star formation in clusters. They also show that sequential harassment will bear an impact depending on where galaxies have resided in a cluster throughout their history. Based on ALFALFA, Hallenbeck et al. (2012) show that some HI-bearing Virgo dEs likely have accreted their gas only recently.

A number of recent studies aimed to identify the threshold in environmental density when gas stripping begins to significantly impact the gas content. Making use

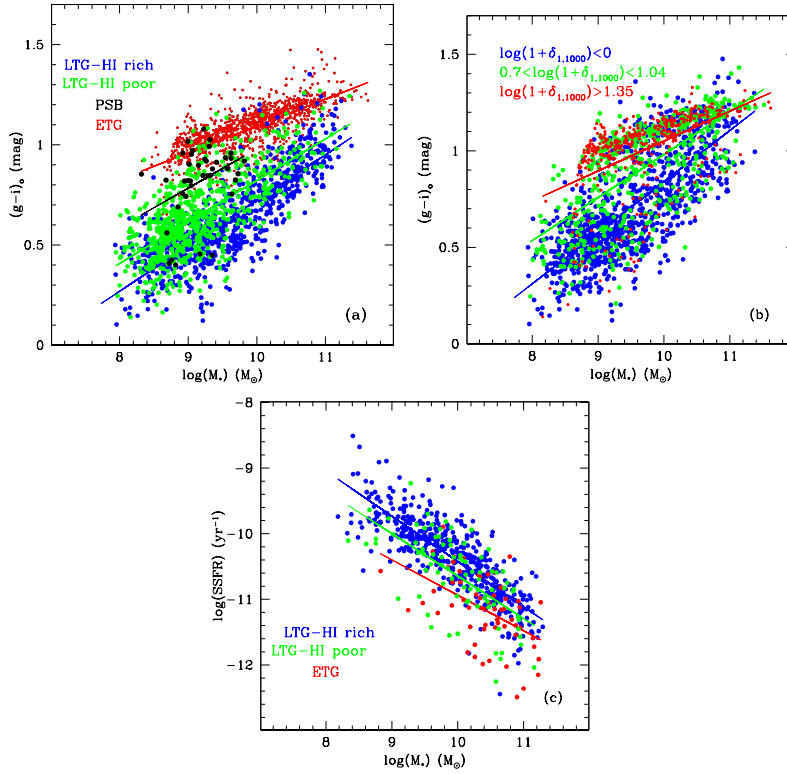


Fig. 9 Four-category sequence in the HI gas-color relationship for galaxies selected on the basis of morphology, gas content and nuclear spectral properties: late type galaxies (LTG) which are HI-rich or HI-poor, post-starbursts (PSB) and early-type galaxies (ETG). From Gavazzi et al. (2013).

of a rich collection of multi-wavelength data from SDSS and $\text{H}\alpha^3$, a narrow band imaging survey of a flux-limited HI sample extracted from ALFALFA, Gavazzi et al (2013) postulate the identification of an evolutionary sequence in galaxies manifesting itself towards progressively earlier morphology, decreasing gas content and decreasing star formation activity, in the neighborhood of rich clusters. In the dwarf regime ($M_* < 10^{9.5} M_\odot$), they identify a four step sequence, from (i) HI-rich late type galaxies, (ii) HI-poor late type galaxies, still exhibiting nuclear star formation, to (iii) HI poor galaxies without either extended or nuclear star formation but with post starburst signature, and (iv) redder early type galaxies showing no gas or star formation on all scales, as shown in Fig. 9. They propose ram pressure as the most likely mechanism in producing this transformation. For Coma, they estimate the infall in the cluster at a rate of approximately 100 galaxies with $M_* > 10^9 M_\odot$ per year.

3.6 The HI view of star formation laws

Star forming galaxies show a tight correlation between their stellar masses and the star formation rate (SFR), known as the “star formation main sequence”. This relation

appears to hold for massive galaxies ($\log M_* > 10$) over at least the redshift range $z < 3$ (Rodighiero et al. 2011; Genzel et al. 2015). In local star-forming galaxies containing various amounts of HI, SF occurs in massive, dusty, dense and cold molecular clouds. So we are faced with the question: Where does the atomic gas fit in? In particular, it is not clear how star formation on sub-kpc scales, strongly correlated with the molecular gas surface density, can lead to the global scaling relations such as those seen in Figure 9.

Kennicutt & Evans (2012) present a thorough review of current understanding of the process of star formation on the scale of galaxies and how star formation couples with the physical characteristics of the interstellar gas. The accumulating body of observational data on the stellar, dust and multi-phase (cold, cool, warm, hot) gas on sub-kpc scales enables tests of the most commonly-used relation between the surface density of star formation and of the gas, the so-called Kennicutt-Schmidt Law $\Sigma_{SFR} \propto \Sigma_{gas}^N$, with $N \sim 1.4$. In combination with the accumulating observational datasets acquired at other wavelengths, HI synthesis maps enable the exploration of the behavior of the spatially-resolved and dust-corrected star formation rate with the changing mix of atomic and molecular gas.

As discussed in detail also by Kennicutt (2010), Schruba et al. (2011) have combined the HERACLES IRAM-30m/CO study with the VLA/HI THINGS to show quantitatively that the atomic and molecular phases relate to star formation in very different ways. Different SF laws appear to apply in different regimes of Σ_{gas} : the HI-dominated medium below $\log \Sigma_{gas} \sim 1 M_\odot \text{ pc}^{-2}$; the H₂-dominated at $1 < \log \Sigma_{gas} < 2.3 M_\odot \text{ pc}^{-2}$, and the starburst regime at higher gas densities: c.f. Fig12 of Kennicutt & Evans (2012). Overall, the HI surface density appears to have little to no impact on the local Σ_{SFR} ; even where the HI dominates, the SFR correlates more closely with the molecular gas. It appears that gas is consumed more rapidly if the molecular fraction is high. The normal process of conversion from atomic to molecular appears to stall in the HI-dominated regions of galaxies, thereby reducing the SF efficiency even in the presence of significant amount of gas.

To first order, the HI-dominance is also reflected in the metallicity of the gas. Low metallicities are seen in dwarf galaxies and the outer disks of late-type spirals. Only in rare instances does CO detection take place in very low metallicity regimes (Elmegreen et al 2013). Since dust grains play critical roles both in hosting the surface formation of molecules and in shielding them from ambient UV photons, it is not surprising that such HI-dominated regions are characterized both by low gas surface-densities ($\Sigma_{gas} < 1 M_\odot \text{ pc}^{-2}$) and higher gas-to-dust ratios. There the global efficiency of star formation $\Sigma_{SFR}/\Sigma_{gas}$ is relatively low and uncorrelated with Σ_{gas} (Bigiel 2008; Kennicutt & Evans 2012). Simulations have shown that H₂ may form even in gas with few or no heavy elements (e.g. Krumholz 2013 and references therein), enabling a path to star formation even in the most unprocessed environments. THINGS and HALOGAS (Heald et al. 2011) have assembled a rich dataset of very deep HI imaging on a growing number of large nearby systems with significant column density sensitivity, to allow searches for in-falling clouds and streams of material. To date, no study has identified accretion at a level sufficient to provide continuous fueling of the current star formation rate. A caveat about these works however reminds us that column density limits can only be quoted for beam-averaged

quantities, that is, under the assumption of a smooth distribution of gas which fills the radio telescope beam and which refers only to the neutral gas. Clumpiness or high fractional ionization can significantly skew the interpretation, or even worse, hide the true gas content. Much work remains to be done, especially at levels of truly low column density and on the smallest scales.

With the advent of the Atacama Large Millimeter Array, studies are just beginning to probe the properties of the bulk of the star-forming galaxies at high redshift. First suggestive studies, notably PHIBSS (Tacconi et al 2013), have begun to explore the redshift range $z \sim 1-2$ using interferometers to identify massive, turbulent gas disks at that epoch. Without the sensitivity of the future SKA, HI studies at this point lag far behind. As a pilot program the HIGH z survey of Catinella & Cortese (2015) have reported direct detections of 39 actively star forming disks at Arecibo, selected from the SDSS, at $z > 0.16$, in observing conditions more RFI-benign than current ones. Interestingly, the HIGH z galaxies are unusually blue and gas-rich, and lie in relatively isolated fields. Catinella & Cortese (2015) argue that they are indistinguishable from the high gas fraction, high HI mass HIGHMass galaxies identified in the ALFALFA survey (Huang et al. 2014; Hallenbeck et al. 2014), but are very different from the PHIBSS molecular-dominated turbulent disks. The HI and H $_2$ populations cannot be linked unless the PHIBSS galaxies contain a large HI reservoir or are not representative of the general disk population at the higher redshifts. It will be a long time before HI facilities have the capability to detect individual galaxies similar to the PHIBSS disks at redshifts > 1 , but the stacking of sources in deep fields such as proposed for the MeerKAT LADUMA project (see Section 6) should provide constrains on the atomic gas content of the turbulent disks.

3.7 The Stellar and Baryonic Mass Functions and Baryonic Deficit

The measurements of the stellar mass/luminosity function (SMF) go back decades (Felten 1977), but only recently wide field, multi-band spectro-photometric optical and near infrared surveys have made it possible to determine the SMF from samples of many tenths of thousands of galaxies (e.g. Baldry et al. 2012 and refs. therein), extending its estimate over the mass range between 10^7 and $10^{12} M_{\odot}$. The low mass end of the SMF is fit by a power law of slope -1.3, in contrast with the steeper power law of index -1.8 predicted by Λ CDM for the halo mass function (HMF).

The technique of ‘‘abundance matching’’ (hereafter ‘‘AM’’; Marinoni & Hudson 2002; Papastergis et al. 2012, 2015 and refs. therein), has been used extensively in the literature, to link the properties of an observed galaxy function, e.g. the SMF, with those of the HMF. By pairing the most massive galaxy with the most massive halo, the second most massive galaxy with the second most massive halo, and so on, AM produces the average function relating stellar mass with halo mass $M_h(M_*)$, i.e. the most likely mass M_h of the halo hosting a galaxy of mass M_* . Several different derivations of that relation are shown in Figure 10 (Papastergis et al. 2012), as solid, dashed or dotted lines. The green filled circles show measurements of the stellar to halo mass ratios; the latter were obtained via stacked weak lensing observations (Reyes et al. 2012); the other symbols are from studies that used kinematic data of individual

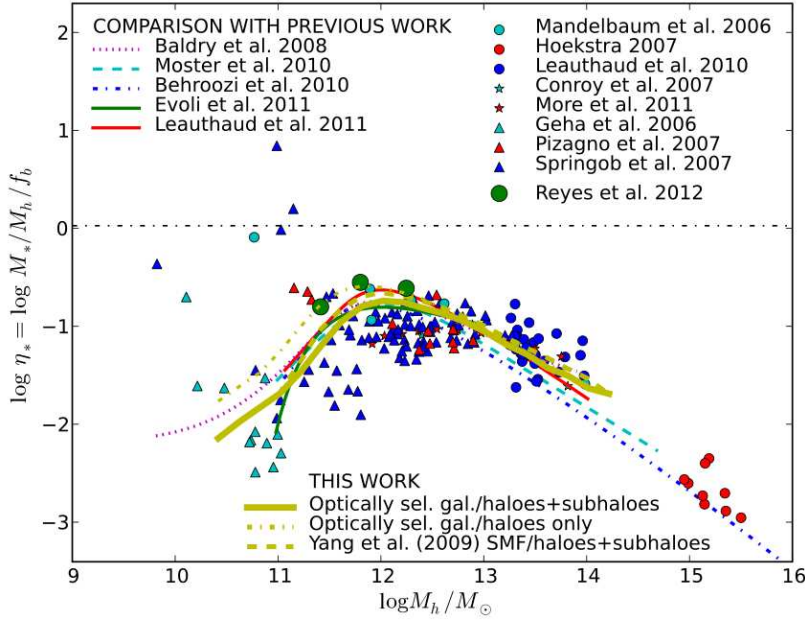


Fig. 10 Logarithm of the ratio of stellar mass to halo mass, plotted as a function of the logarithm of halo mass, normalized by the cosmic baryon fraction. The thick yellow line results from applying the AM technique to the SMF and the HMF. Other dashed or dotted lines correspond to the same function as reported, using AM, in the references listed top left of the figure. The plotting symbols, as listed top right of the figure, identify measurements of the stellar to halo mass ratio whereby the halo mass was estimated by a variety of different techniques. Of particular interest are the three filled, green circle data points, corresponding to measurements of the mean halo mass, via the signature of weak lensing, in the stacked images of three subsets, of several thousand images each (Reyes et al. 2012). Figure credit: Papastergis et al. (2012).

galaxies to estimate halo masses. The y-axis of the plot is $\eta_* = \log[(M_*/M_h)/f_b]$, i.e. the stellar to halo mass ratio is normalized by the cosmic baryon fraction $f_b \simeq 1/6$. Different techniques concur in indicating a relatively low efficiency of galaxies in retaining their baryons, or in converting them into stars, across the full stellar mass spectrum. The fraction η_* of baryonic mass which a galaxy converts into stars is significantly less than one. It peaks near $\eta_* \sim 0.25$ for a (Milky Way-like) halo mass of $\sim 10^{12} M_\odot$, and drops rapidly below 0.1 on both sides of the peak.

Stellar mass, however, is the main baryonic component only in relatively massive systems. The ratio $f_{HI} = M_{HI}/M_*$, where M_{HI} is the HI mass, increases with decreasing stellar mass from its peak, becoming the dominant baryonic component for systems with $M_* < 10^{10} M_\odot$ (Huang et al. 2012a). It is customary to refer to the quantity $M_b = M_* + 1.4 \times M_{HI}$ as the “baryonic mass” of a galaxy, where the factor 1.4 accounts for the Helium mass. We do so, with the understanding that: (i) the molecular mass is a small fraction of the stellar mass when $M_* > M_{HI}$ and it is a small fraction of the atomic gas mass when $M_* < M_{HI}$ (Saintonge et al. 2011), and (ii) the mass of a hot corona may be the dominant — but generally not measured — baryonic component in massive systems. Figure 11 shows the correction from η_* (the

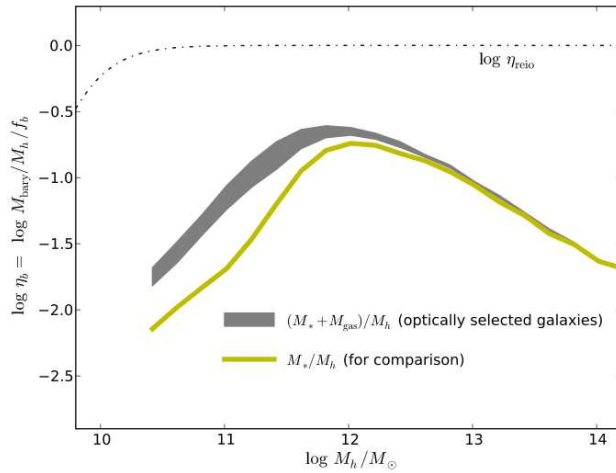


Fig. 11 In grey shading, the logarithm of the ratio of baryonic to halo mass is plotted as a function of the logarithm of halo mass, normalized by the cosmic baryon fraction. For comparison, the yellow line shows the ratio of stellar to halo mass, same as in Figure 10. Figure credit: Papastergis et al. (2012).

thick yellow line), to η_b , the value inclusive of both stars and atomic gas (the grey shaded region, after Papastergis et al. 2012).

Optically dark and almost dark HI sources are detected by ALFALFA, alleviating the baryon deficit from the magnitude shown by the yellow line in Figure 11 to that indicated by the grey one. However, that alleviation is not sufficient to overcome most of the observed baryonic deficit, as we discuss further in Section 5.

Having directly measured HI masses for each individual galaxy in the derivation of the baryonic mass function is important. Obtaining an indirect estimate of the cold gas in galaxies by using an average scaling relation between M_{HI}/M_* and M_* , Baldry et al. (2008) inferred that the increasing gas fraction in dwarf galaxies should approximately offset the decreasing stellar-to-halo ratio and should result in a roughly constant, bottom-line $\eta_b \simeq 0.1$. This spurious result would have implied that dwarf galaxies are relatively efficient at retaining baryons, but very inefficient at converting them into stars. As indicated by Kochanek & White (2001) and Sheth et al. (2003), this approach is vulnerable; in this case leading to erroneous inferences on the derived baryonic mass function. The direct measurement of the baryonic mass made possible by an HI survey circumvents this vulnerability.

4 (Almost) Optically-Dark Extragalactic HI sources

An important feature of the ALFALFA data releases is the identification of a most probable optical counterpart of each HI source, a task performed as an integral part of the process of ALFALFA catalog construction (c.f. Haynes et al. 2011). Although the vast majority of HI line sources detected by ALFALFA can be clearly identified with an optical counterpart, about 6% appear to be optically-“dark” vis-a-vis public, wide field data bases such as SDSS. A large fraction of those includes the long-known

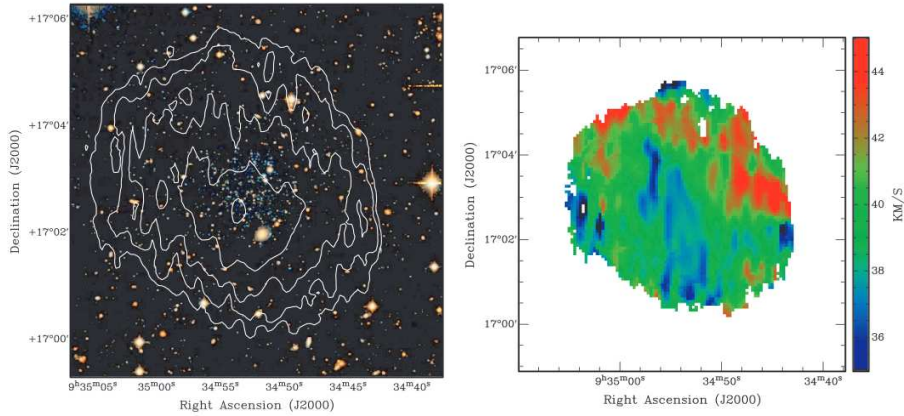


Fig. 12 **Left:** Integrated HI synthesis image of Leo T (HI column density contours at 2.5 , 10 , 20 and $50 \times 10^{19} \text{ cm}^{-2}$), superposed on a deep g - and r - image. **Right:** Velocity field of Leo T from WSRT data. A hint of rotation? Credit for both panels: Ryan-Weber et al. (2008)

high velocity HI clouds (HVCs), a subset of which are the ultra-compact high velocity HI clouds (UCHVCs). Excluding HVCs, some of which may be extragalactic as we discuss in section 4.1, the extragalactic but dark ALFALFA detections amount to about 1% to 2% of the full catalog. Sources in this small subset fall in three categories: (i) the spectral line does not arise from an HI transition but rather one of OH megamasers at redshifts near $z \sim 0.2$ (Darling & Giovanelli 2002; Suess et al. 2015), (ii) tidal appendages of gas-rich galaxies or remnants of ram pressure events in clusters and (iii) “something else”. The source count for the latter category adds up to several dozens. Their classification as optically-dark in the ALFALFA catalog is based on examination of the SDSS and DSS2 optical images in the vicinity of the ALFALFA HI centroid. In some cases, a faint, low-surface brightness stellar counterpart may be visible in deeper images than provided by the public surveys; hence the modifier “almost-dark” is adopted. We discuss UCHVCs and objects in category (iii) respectively in sections 4.1 and 4.2.

4.1 Ultra Compact High Velocity Clouds (UCHVCs)

The idea that compact HVCs may represent the baryonic counterparts of low mass dark matter halos, undetected by optical surveys but located within or in the near vicinity of the Local Group, was first proposed in two influential papers by Blitz et al. (1999) and Braun & Burton (1999). However, the compact HVCs identified as possible candidates extracted from early, low resolution surveys failed to qualify: if located at Mpc distances, they would strongly violate the Λ CDM mass/concentration relation and should have been, but were not detected by extant surveys of nearby galaxy groups (Pisano et al. 2008, Sternberg et al. 2002). The idea was reconsidered more recently (Giovanelli et al. 2010; Adams et al. 2013), as ALFALFA’s angular

resolution allowed detection of even more compact HVC sources than available in the 1990s, labeled ultra-compact HVCs. Convincingly proving that an ALFALFA UCHVC is indeed the baryonic counterpart of a low mass dark matter halo is difficult. It requires higher HI angular resolution maps than provided by ALFALFA ($\sim 4'$), in order to identify a possible rotationally supported disk and/or some indication of distance, e.g. through the detection of an optical counterpart which would be fainter than the limit of extant optical surveys but bright enough to resolve individual stars.

Leo T was found as a stellar overdensity in the SDSS (Irwin et al. 2007). Follow-up HI synthesis observations with the GMRT and the Westerbork arrays (Ryan-weber et al. 2008) revealed an HI counterpart with a heliocentric velocity of 35 km s^{-1} , also detected by HIPASS and ALFALFA, which would have found it to be a good UCHVC candidate. At an estimated distance of 420 kpc, its HI mass is $2.8 \times 10^5 M_{\odot}$, its stellar mass is $0.7 \times 10^5 M_{\odot}$, its HI radius is 0.3 kpc and the dynamical mass is $> 3.3 \times 10^6 M_{\odot}$. Its color-magnitude diagram shows evidence of two episodes of star formation: a currently ongoing one, of approximate age of 200 Myr, as well as an older one, aged 6–8 Gyr. Figure 12 (left panel) shows HI column density contours at the levels 2.5, 10, 20 and $50 \times 10^{19} \text{ cm}^{-2}$, superimposed on a g - and r - image, while the right panel shows the velocity field.

AGC 198606, also known as “friend of Leo T”, is an ALFALFA-discovered UCHVC located 16 km s^{-1} and 1.2° from Leo T. No optical counterpart has yet been found, but HI synthesis imaging with WSRT shows signature of a rotating disk with $V_{rot} \simeq 14 \text{ km s}^{-1}$ (Adams et al. 2015). Its distance is not yet known. Assuming that it is located at 420 kpc, the same distance of Leo T, it would have an HI mass of $6.2 \times 10^5 M_{\odot}$, an HI radius at the $5 \times 10^{18} \text{ atoms cm}^{-2}$ isophote of 1.4 kpc, a dynamical mass within that radius of $1.5 \times 10^8 M_{\odot}$ and an upper limit for its i' -band absolute magnitude of -6.6.

Leo P was discovered by ALFALFA and cataloged as an UCHVC. In the SDSS it appears as a faint, irregular, lumpy feature, identified as a compact group of galaxies by McConnachie et al. (2009). However, deep imaging with the WIYN telescope resolved the optical emission into stars and a bright HII region, likely ionized by an O7V or O8V of about $25 M_{\odot}$ mass. Leo P is located 1.6 Mpc away (McQuinn et al. 2015), has a stellar mass of $5.7 \times 10^5 M_{\odot}$ and an HI mass twice as high, an HI radius of half a kpc, a dynamical mass of $2.3 \times 10^7 M_{\odot}$ within that radius and $(12 + \log(O/H) = 7.16 \pm 0.04)$ (Giovanelli et al. 2013, Rhode et al. 2013, McQuinn et al. 2013), making it the lowest metallicity, star forming galaxy known in the Local Volume (Skillman et al. 2013). With a heliocentric radial velocity of 264 km s^{-1} , it lies in the near periphery of the Local Group. The best-fitting star formation history favors “star formation at the earliest epochs, followed by a period of quiescence and a relatively constant star formation rate at recent times” (McQuinn et al. 2015). HI imaging with the VLA and GMRT revealed a rotating disk with $V_{rot} \simeq 10 \text{ km s}^{-1}$ (Bernstein-Cooper et al. 2014). Figure 13 shows VLA-C HI integrated column density contours superimposed on an optical image taken with the WIYN telescope (left hand panel) and the location of Leo P in the baryonic TF relation (fuzzy symbol; right hand panel). This source is a confirmed dwarf galaxy within a minihalo. Had it been ~ 2.5 times farther away, it would not have been detected by ALFALFA.

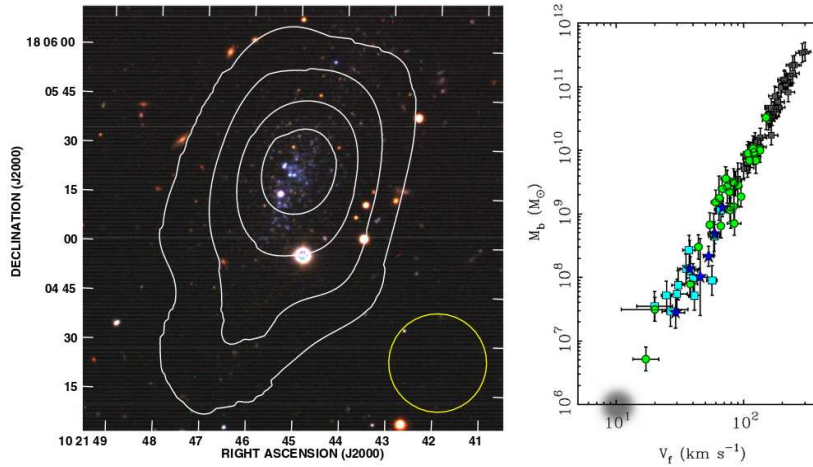


Fig. 13 Left: VLA-C integrated HI synthesis image of Leo P (HI column density contours at 0.5 , 1 , 1.5 and $2.0 \times 10^{20} \text{ cm}^{-2}$) smoothed to an angular resolution of $30''$ (yellow circle), superimposed on the WIYN telescope image. **Right:** Location of Leo P (fuzzy symbol) on the baryonic TF relation. Both figures from Giovanelli et al. (2013), the latter adapted from McGaugh (2012).

4.2 Two Examples from the Gallery of Darks

By definition, the baryonic component of systems of category (iii), “something else” is dominated by atomic gas, rather than by stars. To add to their exceptionality, some of these systems are not “minihalo” candidates such as Leo P and Leo T: their HI masses can rival that of the Milky Way. However, their HI linewidths tend to be quite narrow, typically $< 50 \text{ km s}^{-1}$ full width at half power, similar to that seen in dwarf galaxies. These strange almost-dark ALFALFA sources appear to have been unable to deliver a sustained star-formation rate (SFR) at a level that would be compatible with their gas content. There is a well-known mismatch between the expected SFR of a galaxy, as assessed from the masses of giant molecular clouds gauged to reach collapse, and its observed SFR. In the case of the Milky Way, the mass of giant molecular clouds and their estimated free-fall times would yield a current SFR of $\sim 250 M_{\odot} \text{ yr}^{-1}$, sustainable over several Gyr, yet the observed SFR is ~ 100 times lower (Zuckerman & Evans 1974; McKee & Williams 1997). Similar results have been obtained by Wong & Blitz (2002) for a sample of nearby galaxies. Theoretical studies indicate that the solution of the problem might invoke regulation by turbulence, an approach that appears also to explain scaling relations such as the Kennicutt–Schmidt law (Krumholz & McKee 2005 and references therein). The objects with extreme $M_{\text{HI}}/L_{\text{opt}}$ being detected by ALFALFA exacerbate that mismatch. As a case study, the pair of almost dark objects named AGC 229384/5 is described next.

The left panel of Figure 14 displays the WSRT HI column density contours superimposed on an optical image of a field containing several ALFALFA sources. The optical image is a composite of three 45-min exposures in filters (g , r and i) made with

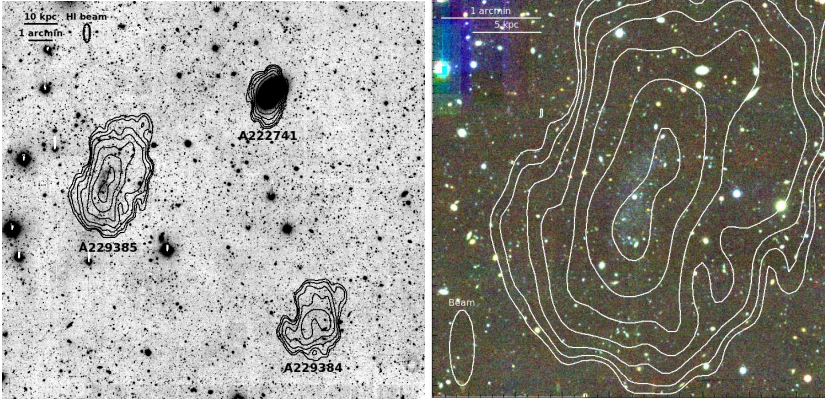


Fig. 14 **Left:** A deep g , r and i composite image of a $12' \times 12'$ field containing a pair of almost-dark ALFALFA sources. Superimposed are the contours of the HI column density obtained with the WSRT, at 1, 2, 4, 8, 16, 32, and $64 \times 10^{19} \text{ cm}^{-2}$. Three HI sources are clearly detected. Two of them (labelled AGC 229384 and AGC 229385) are at cz of respectively 1309 and 1348 km s^{-1} ; the third, AGC 222741, is an undisturbed background spiral at $cz = 1844 \text{ km s}^{-1}$. **Right:** A $4' \times 4'$ blow up centered on AGC 229385, showing a faint, blue optical counterpart coincident with the HI source. AGC 229384 has no optical counterpart. Credit: Janowiecki et al. (2015).

the pODI camera at the 3.5m WIYN telescope (Janowiecki et al. 2015). The strongest HI source is an undisturbed background spiral (CGCG 129-006 = AGC 222741) at $cz=1844 \text{ km s}^{-1}$. The other two are in the foreground and have no SDSS counterpart.

While AGC 229384, at $cz = 1309 \text{ km s}^{-1}$, has no detected optical counterpart even in the composite WIYN image, AGC 229385, at $cz = 1348 \text{ km s}^{-1}$, has a faint, blue stellar counterpart of $g = 19.27$ and peak g surface magnitude of $26.6 \text{ mag arcsec}^{-2}$, evident in the zoomed up right hand panel of Figure 14. A flow model which accounts for local inhomogeneities of the cosmic density field yields a most probable distance of $\sim 25 \text{ Mpc}$ for the two objects, although in this region, projected not far from the virial radius of the Virgo cluster, the uncertainty on the distance error may be as high as 50%. The properties of both (almost) dark objects are extreme. With $M_{HI} = 10^{8.8} M_{\odot}$, only a few times smaller than that of the Milky Way, AGC 229385 has a $M_{HI}/L_g = 44$, and a stellar mass of only $\sim 10^7 M_{\odot}$. Moreover, with a linewidth $W_{50} = 34 \text{ km s}^{-1}$ and an HI radius of 14 kpc, the dynamical mass within that radius, $M_{dyn} = 10^{9.0} M_{\odot}$, is comparable to that of its HI mass. Were it not for its current star-forming activity, AGC 229385 might have escaped optical detection altogether. At 25 Mpc, HI mass, radius and linewidth for AGC 229384 would be respectively $10^{8.3} M_{\odot}$, 7 kpc and 27 km s^{-1} ; the dynamical mass within the HI radius would be $10^{8.5} M_{\odot}$. The apparent shallowness of the potential well of these two sources is exceptional, given their size. Small tidal disturbances would be able to remove much of their gas, so their current properties may be made possible by their relative isolation. A suggestive possibility would describe them as long quiescent, low mass halos, recently rejuvenated by accretion of a substantial mass of

intergalactic gas, just conducive to starting a star-forming episode. As hypothesized by Salpeter & Hoffman (1995) in explaining the low redshift Ly α absorbers, these may be “vanishing Cheshire cat” galaxies.

5 Missing Satellites, etc.: Too Big To Fail?

Klypin et al. (1999) and Moore et al. (1999) noted a deficiency in the number of low mass galaxies (satellites) found within the halo of the Milky Way (MW), with respect to the number of subhalos predicted by Λ CDM. Hence the tag “missing satellites problem” arose. Furthermore, Boylan-Kolchin, Bullock & Kaplinghat (2011) noted that some of the MW subhalos predicted by Λ CDM/AM — where AM is the Abundance matching technique discussed in section 3.7 — are significantly more massive than any of those observed, hence suggesting the paradox that the MW is missing a population of subhalos TBTF: “too big to fail”. Were the TBTF phenomenon be noted in the MW alone, its occurrence could be attributed to small number statistics. However, more recently Tollerud et al. (2014) have shown that M31 also has a TBTF problem; in fact, Ferrero et al. (2012) and Papastergis et al. (2015) showed that the population of field dwarfs do so as well. The latter is an important result, since the environmental conditions of field dwarfs — which are among the most isolated of galactic systems in the Universe (see section 3.1)— are very different from those within the virial radius of a galaxy as massive as the MW. The paucity of low mass galaxies, in comparison with the abundance of low mass halos predicted by Λ CDM, has been known for a long time, appearing in a variety of guises, e.g. as the “void phenomenon” (Peebles 2001) and in the derivation of luminosity, HI mass, rotational velocity functions (Baldry et al. 2008; Klypin et al. 2014; Zwaan et al. (2010) Papastergis et al. 2014 and references therein). The simplest and most direct scenario for the investigation of the connection between observations and Λ CDM predictions is that offered by the rotational velocity function. It presents the least intrusion by baryonic physics processes, both it and the halo velocity responding to the radial distribution of mass. Because the HI gas extends radially farther than any other directly observable component, the observed rotational velocity gets as close to the halo velocity as it gets.

The cumulative velocity functions of the $\alpha.40$ sample of the ALFALFA survey, vis-a-vis the halo Velocity function, are shown in the left panel of Figure 15, respectively by the green solid line and the black solid line. The average relation $V_h(V_{rot})$, as derived via the AM technique, is shown by the blue line in the right panel of the figure. The two velocity functions roughly track each other for velocities greater than $\sim 60 \text{ km s}^{-1}$, but part decisively at velocities lower than that. In the derivation of the velocity function of the HIPASS survey, Zwaan et al. (2010) reported the mismatch to take place for velocity widths $< 100 \text{ km s}^{-1}$, although with greater uncertainty than yielded by ALFALFA’ $\alpha.40$, as the latter includes $\simeq 8\times$ as many detections of low mass sources as the HIPASS catalog (cf. Section 3.2). The $V_h(V_{rot})$ relation inferred via AM predicts that galaxies with $V_{rot} \sim 15 - 20 \text{ km s}^{-1}$ reside in halos with $V_h \sim 40 - 45 \text{ km s}^{-1}$; halos with $V_h < 40 \text{ km s}^{-1}$ would be expected not to host any galaxies at all.

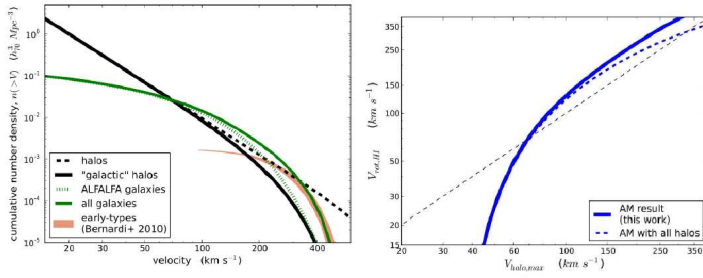


Fig. 15 Left: The solid black line is the Λ CDM cumulative number density of halos as a function of their maximum circular velocity V_f , as derived from the Bolshoi simulation. The solid green line is the cumulative number density of ALFALFA galaxies’ plotted as a function of their rotational velocity V_{rot} . **Right:** The blue line is the average relation between V_h and V_{rot} , as obtained via AM; the dashed black line is merely for 1-to-1 reference. Ignore the other lines. Credit: Papastergis et al. (2015).

In an effort to verify the prediction of Λ CDM/AM, Figure 16 shows a preliminary result displaying the distribution of 194 galaxies with resolved, interferometric HI rotation curves, in a V_h vs V_{rot} plot (symbols and colors identifying data sources as coded within the plot). These data allow an independent estimate of the most massive Navarro-Frenk-White (NFW) halo compatible with the V_{rot} at the last measured point of the rotation curve, i.e. they allow a determination of an upper limit of $V_{halo,max}$ for each galaxy, and thus to test the Λ CDM/AM predictions. The solid blue line in Figure 16 is the same function as displayed in the right hand panel of Figure 15, i.e. the locus of the Λ CDM predicted relation V_h/V_{rot} , as delivered by AM. The value of V_{rot} for each galaxy is inferred from the last measured point of the rotation curve, corrected for inclination; the value of V_h (labelled in the Figure as $V_{halo,max}$) is that of the most massive NFW halo compatible with the V_{rot} at the last measured point of the rotation curve, i.e. each $V_{halo,max}$ is an upper limit. The test, as shown in Figure 16, fails to confirm the Λ CDM prediction. The steep downturn predicted by AM, for velocities lower than about 60 km s^{-1} is not compatible with the observed data. The halos hosting galaxies with $V_{rot} < 30 \text{ km s}^{-1}$ appear to have significantly lesser values of V_h than predicted by Λ CDM/AM.

The steep slope of the predicted relation V_h/V_{rot} between $V_h \simeq 40$ and 60 km s^{-1} raises another issue. Low velocity galaxies with $V_{rot} < 50 \text{ km s}^{-1}$ would “crowd” over a narrow range of halo velocities. One would thus expect a change in the slope of the baryonic Tully-Fisher relation, becoming shallower for $V_{rot} < 50 \text{ km s}^{-1}$. That does not seem to be the case, as shown in Figure 13,

For the Λ CDM/AM approach to yield predictions more closely compatible with observations in the low end regime, it would be necessary (i) to either increase the low end slope of the VF or (ii) to reduce the low end slope of the halo VF. Option (i) would require counting galaxies of low V_{rot} which so far have been missed by surveys, while option (ii) requires hiding halos by making their baryons invisible. The burden in correcting the mismatch between the galaxy and halo cumulative velocity functions near the low velocity end is a heavy one. Warm, rather than cold DM particles with mass of few keV, could suppress structure on small scales and lower the counts

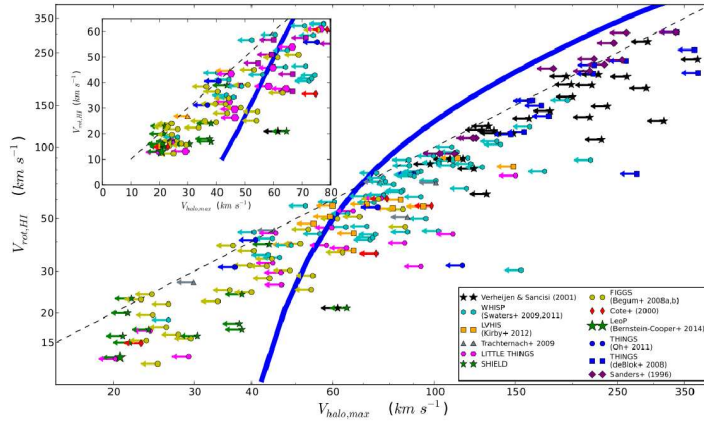


Fig. 16 Distribution in a V_h vs V_{rot} of 194 galaxies with resolved, interferometric HI rotation curves. The solid blue line is the same function as displayed in the right hand panel of Figure 15. The V_{rot} value is the velocity as given by the last recorded data point of the rotation curve of each galaxy, after correction for disk inclination and turbulence; the V_h value is the maximum velocity of the most massive halo compatible with the galaxy’s rotation curve. The inset panel is a zoom-in, in linear axes, of the low velocity region of the larger diagram. Credit: Papastergis et al. (2015).

of small halos. This is a radical approach, which may however fail other astrophysical tests (Papastergis et al. 2015). Less radical solutions may exist. Λ CDM simulations of high resolution and inclusive of the treatment of fully implemented baryonic processes may reveal modifications of the properties of low mass halos that would reduce their visibility and thus reduce small halo counts. In a recent review, Pontzen & Governato (2014) underscored the importance of this solution (see also Governato et al. 2010 and 2012). Brooks & Zolotov (2014) and Sawala et al. (2014) have shown that proper account of supernova feedback and tidal stripping of subhalos by the interaction with the central galaxy’s halo can match the observed properties of the MW and M31 satellites, and thus explain the TBTF problem in those two systems. However, some of these processes depend on the vicinity of a massive galaxy, and can explain the TBTF syndrome in MW and M31 subhalos, but should be less important in the field. It thus remains unclear whether full hydrodynamical simulations can save the day for Λ CDM in low galaxy density environments.

Inspection of Figure 16 shows that low mass halos detectable at 21cm, albeit not abundant, do exist. Examples of such a population are discussed in section 4: Leo P was detected by ALFALFA, which motivated a search for an optical counterpart (Section 4.1); like AGC 229385 (Section 4.2 it is undergoing a mini-starburst. It is located 1.7 Mpc away; it would not have been detected if it were $\simeq 2.5\times$ farther away. Likewise, AGC 229385 is also undergoing a mini-starburst; its distance is uncertain, but it appears to reside within a low mass halo. The same holds for its companion, AGC 229384, which has no optical counterpart. Although several other objects with similar properties are detected by ALFALFA, the whole detected lot of “almost dark” sources is not sufficient to account for more than a tiny fraction of the mismatch evidenced in

Figure 15. Could other objects exist, more abundant but just below the depth of the current surveys?

5.1 Too Shy to Shine

Geha et al. (2012) recently made a discovery of high relevance to the TBTF issue. Extracting a sample of dwarf galaxies from the SDSS spectroscopic data base (objects of stellar mass M_* between 10^7 and $10^9 M_\odot$), they queried what fraction of that population is currently star forming. A galaxy was classified as star forming if $H\alpha$ emission is detectable and there is evidence of a strong 4000\AA break. Two subsamples were drawn according to a simple environmental criterion: the projected distance to the nearest massive galaxy. If that distance is greater than 1.5 Mpc, the dwarf object is part of the “field” population. By these criteria, they found that more than 99% of 2951 field dwarfs are currently forming stars.

This finding is surprising, since the history of star formation in dwarf galaxies is thought to be episodic (Tolstoy et al. 2009) with a typical duration of starburst events in dwarfs of 200 to 400 Myr (McQuinn et al. 2009). If the typical field dwarf is star-forming for only a fraction of the time, a complementary fraction of field dwarfs must be in a quiescent state. If the average field dwarf has only a few starbursting episodes over a Hubble time, the uncounted, dormant field dwarfs could account for the missing objects responsible for the steep drop in the V_{rot} vs. V_H relation in Figure 16.

Halos of mass lower than $\sim 10^{10} M_\odot$ ($V_h \sim 30 \text{ km s}^{-1}$) may have been able to form stars before reionization, but unable to accrete fresh gas from the IGM and thus to form stars after reionization (Hoeft et al. 2006). However gas accretion and star formation may have become possible at later epochs, especially in low density environments (Ricotti 2009). In fact some do now. These items of evidence would suggest that between star formation episodes field dwarf galaxies can be dark, their optical and HI emissions being quenched. The histories of star formation of nearby dwarf systems would suggest that the fraction of such objects — unaccounted by surveys and TSTS (too shy to shine) — is large. A similar conclusion has been reached by Kormendy & Freeman (2014,2015) in their investigation of the scaling laws of dark matter halos in late-type and dwarf spheroidal galaxies.

And the skies may be crowded with low mass halos, ready — like Salpeter & Hoffman’s (1995a,b) “Cheshire Cat” — to modestly shine.

6 The HI Frontier: Tracing HI over Cosmic Time

While the low redshift surveys provide measures of the fundamental relations between stars, atomic gas and dark matter in the current galaxy population, future efforts will aim to explore how the HI content evolves along with the stellar and molecular components over cosmic time. At the time of this review, we find the field of HI surveys poised to exploit new facilities offering huge advances in bandwidth and field of view, leading to a future revolutionary instrument, the Square Kilometre Array. Here

we discuss the benchmarks that are likely to define the surveys that will take place in the next years and then by outlining representative ones that are on-going or planned as of now.

6.1 Designing Future HI Surveys: The Telescope Figure of Merit

New facilities are being designed or under construction, which will be used to carry out ambitious HI surveys in the next decade. In this section we briefly visit the announced characteristics of the telescopes and an even briefer one of some of the surveys which will dramatically expand our view of the HI Universe. A useful parameter often used for the comparison of telescopes and surves is a Figure of Merit (FoM)

$$FoM \propto (A_{eff}/T_{sys})^2 \Omega_{fov} BW \quad (8)$$

where A_{eff} is the telescope aperture efficiency, T_{sys} the system temperature of the receiver, Ω_{fov} is the solid angle of the telescope field of view and BW is its spectral bandwidth.

Assume arbitrarily a unit FoM corresponding to an Arecibo-like telescope with an $A_{eff} \simeq 4 \times 10^4 m^2$, a $T_{sys} = 25$ K and a single pixel field of view. Then the same telescope operating over the same bandwidth with a 7-feed array and a degraded T_{sys} of 31 K, as would be the Arecibo telescope with the ALFA focal plane array, would have a $FoM = 4.7$. FAST, an Arecibo-like telescope currently under construction in southern China, will gain by a factor 3 in A_{eff}^2 , and with a 19 feed planned focal plane array it should yield a $FoM \simeq 39$, a huge gain over Arecibo. MeerKAT, under construction in South Africa, will be a "traditional" synthesis array of 64 antennas while Apertiv and ASKAP, respectively operating in Holland and Australia, will be arrays of between 24 and 36 telescopes, each getting a big kick in FoM by the installation of focal plane phased arrays (FPPAs) in each of its antennas. While the T_{sys} performance of FPPAs is still somewhat uncertain, the multiplexing advantage of the FPPA technology is extraordinary and should pay back handsomely. Plans at Arecibo and FAST are also afoot for the construction of respectively 40 and 100 beams FPPAs. At these single dish facilities, optimizing the performance of a single FPPA by, e.g., cooling the unit, may allow achieving a T_{sys} below 50 K.

Important concerns not contemplated by the FoM as defined above include the impact of RFI and source confusion, as well as the fact that interferometric arrays will make it possible to spatially resolve HI sources out to much larger distances than will AO and FAST.

As discussed in Section 2.3 and above, RFI is a serious impediment as future surveys explore further into the universe and the redshifted HI line shifts to lower and lower frequencies where RFI threatens to become a limiting factor. Interferometers are less prone to the impact of transient or time-varying RFI as the path length to individual elements of an array varies. However, receiver saturation will induce bad array data and therefore can have a serious impact even on interferometric surveys. While some telescope sites are located far from urban areas in "radio quiet" zones, satellite transmissions are increasingly rendering bands entirely unusable, regardless

of Earth location. Alert monitoring, identification of RFI sources and legal protection are increasingly important.

Another critical issue for the design of future surveys to measure possible evolution of the HI mass function is the impact of source confusion (Duffy et al. 2012; Delhaize et al. 2013; Jones et al. 2015a, 2015b). While the addition of the velocity dimension reduces the impact of confusion on spectral line surveys, confusion will be particularly critical for future surveys with single dish telescopes like Arecibo and FAST. Because of their large beams, confusion will start becoming a problem at moderate redshifts. Source confusion may also constrain some of the future deep surveys with synthesis arrays, particularly if full angular resolution is not achieved. In general, the impact of confusion on the derivation of the HI mass function and its evolution with z is to increase the derived value of the knee-mass M_* and to steepen the faint end slope α . The forte of the large aperture single dishes will be the relatively nearby universe, where their sheer detection sensitivity will allow the detection of objects to very low HI mass, enabling studies of the faint end of the HI mass function to $\log M_{HI}/M_\odot \sim 10^6$. On the other hand, the wide shallow interferometric surveys WALLABY and WNSHS (see Table 3) will be only negligibly affected by confusion. Confusion will also have an impact on the potential of survey data bases to be mined with the stacking technique, as discussed in Section 2.4. Jones et al. (2015b) show that the stacking potential of DINGO UDEEP will be affected if ASKAP is unable to achieve a resolution of $10''$ for that experiment. In principle, ASKAP should be able to deliver the higher resolution if sufficient computational power is available to the DINGO UDEEP program. Due to their planned angular resolution, CHILES and LADUMA (see Table 3) should be relatively unaffected by confusion.

6.2 Current and Planned Interferometric Surveys

In preparation for the deployment of the SKA pathfinders (Arecibo-AO40, FAST, WSRT/APERTIF, ASKAP and MeerKAT), a number of pilot programs to search for HI in emission at higher redshift have been recently undertaken or are underway. Table 2 summarizes the main characteristics of recent and on-going pilot studies which are opening the HI window into intermediate redshifts while the current plans for some of the pathfinder surveys are presented in Table 3.

6.2.1 HI Emission beyond the Local Universe: First Results

Exploiting the huge collecting area of the Arecibo telescope, the pointed HIGHz program of Catinella & Cortese (2015) detected HI emission from 39 actively star-forming spirals at $z > 0.16$. The targets were selected from the SDSS database on the basis of their optical morphology (well formed, non-interacting disks) and H α line emission (modest H α equivalent width). As selected, these are relatively isolated, massive gas-rich disks, all with HI masses of $2 - 8 \times 10^{10} M_\odot$, stellar masses $2 - 22 \times 10^{10} M_\odot$, and SFRs of $3-35 M_\odot \text{ yr}^{-1}$. While they have unusually high HI gas fractions and very blue (NUV-r) colors, their gas content is *not* unusual given their

Table 2 Representative Pilot HI Emission Studies at Higher Redshift

Survey	Selection	z	N_{det}	Ref
HIGHz	targeted SDSS-selected spirals	0.17-0.25	39	^a
GMRT/A 370	field of cluster A 370 [†]	0.37	†	^b
GMRT/Cosmos	single pointing, zCosmos field [†]	0.345-0.387	†	^c
BUDHIES/WSRT	fields of clusters A 963 and A2192	0.16-0.22	150	^d
CHILES-pilot	single pointing of COSMOS field [†]	<0.193	33	^e

[†] stacking technique used to derive average properties of optically selected samples

^a Catinella & Cortese (2015)

^b Lah et al. (2009)

^c Rhee, J., Briggs, F.H., Lah, P., Chengalur, J.N. (in prep)

^d Verheijen et al. (2007); see update discussed in Jaffé et al. (2013)

^e Fernández et al (2013)

UV and optical properties. This result suggests that the galaxies are the higher redshift analogues of the most massive and largest disks found in the ALFALFA-selected HIghMass sample by Huang et al. (2014) and in fact have HI depletion timescales on the order of ~ 3 Gyr, typical of those found in normal star forming galaxies locally. Despite their large HI masses and the large collecting area of Arecibo, typical integration times for these detections amounted to 2-4 hours ON-source (typically less than one half of the total time per target including bandpass subtraction but not accounting for data rejected because of RFI or standing waves). The sensitivity required to detect the very weak HI signals from distant galaxies remains a challenge.

The SKA pathfinder arrays will be largely dedicated to the conduct of legacy surveys, including ones devoted to detecting the HI line or targeting the well-known “deep field” for which large multiwavelength datasets enable the use of the stacking techniques discussed in Section 4. For several of these programs, no HI was detected from individual objects, but limits on the aggregate are set via the stacking of signals at the 3-d positions of optically-known galaxies. But the detection of individual targets is beginning to pick up. Verheijen et al. (2007) report the detection of 42 galaxies at $z \sim 0.2$, in a pilot of the BUDHIES/WSRT survey; more recently Jaffé et al. (2013) update that number to 150. The combination of stacking and individual detection has permitted Verheijen et al. (2007) to suggest that the blue galaxies in Abell 963 are relatively HI poor compared to similarly blue disks outside the cluster. And, as a concept demonstration of the potential for really deep interferometric HI imaging, the CHILES pilot program (Fernandez et al. 2013) exploited 50 hours with the Very Large Array to search a $34 \times 34'$ region of the COSMOS field at $0 < z < 0.193$. The pilot experience yielded detection of 33 galaxies, 30 of which had been detected spectroscopically at optical wavelengths. These programs have been intended mainly to demonstrate the efficacy of techniques and predicted outcomes of much more significant investments of telescope time with telescope arrays, and have successfully made their point.

6.2.2 HI Absorption Studies

An alternative approach to the study of the hydrogen content of distant objects, mentioned only briefly here, relies on the detection of HI in absorption, either in the HI 21cm line in the direction of strong radio continuum sources or as Lyman- α absorption in the spectra of distant quasars. Unlike flux-limited HI emission line studies which are mass-limited at any distance and reflect both the cold and warm gas, absorption line detection is column-density limited (at fixed continuum strength) and therefore distance-independent and most sensitive to the cold gas in galaxies (Rao & Briggs 1993). Absorption line studies probe the HI environment in the direction of strong radio sources with absorption detected both in close association with the radio source (“intrinsic absorbers”, e.g. Roberts 1970; Curran et al. 2013;) and in absorbers along the line of sight to the background source (“intervening absorbers”, e.g., Brown & Roberts 1973; Roberts et al. 1976; Tanna et al. 2013; Kanekar 2014). Such measurements, in combination with multiwavelength studies of other tracers, provide a powerful probe of the environments of strong radio sources and, in the small fraction that arise from intervening absorbers, the cosmic mass density of neutral gas in Damped Lyman α (DLA) at different redshifts. Nearly all measurements of the latter come from optical observations of the redshifted Ly α absorption along lines of sight to background QSOs (e.g. Wolfe et al. 1986, Prochaska & Wolfe 2009, Noterdaeme et al. 2012).

However, additions to new bandwidth capabilities of the GMRT and JVLA and the wide area coverage of new surveys is enabling a new generation of HI absorption line studies. Samples of HI synthesis mapping of intrinsic absorbers are growing (e.g. Chandola, Gupta & Saikia 2013; Gereb et al 2015a,b). The synthesis maps yield both the structure of the underlying continuum source and the kinematics of the gas. In some cases, the signature of gas infall onto the active nucleus (e.g., Srianand et al. 2015) is evident, while in others, outflows are more likely (Gereb et al. 2015b). Future systematic studies will explore the causal relationships between HI absorption and the impact of mergers and feedback.

Making use of an early version of the ALFALFA dataset, Darling et al. (2011) discuss the potential to use the future wideband capabilities of the SKA pathfinders to look for the HI analogues of DLA absorbers. A first demonstration of the power of these future surveys using the Australian SKA Pathfinder (ASKAP) searched the full redshift range $0.4 < z < 1.0$, yielding a new detection at $z = 0.44$ (Allison et al. 2015) in anticipation of the proposed ASKAP/FLASH survey. Over the next years, FLASH will use the 300 MHz capability of ASKAP to search for HI absorbers both in the radio source hosts and in intervening absorbers, starting as ASKAP early science with targeted fields. The MeerKAT Absorption Line Survey (MALS) will survey the entire bandwidth from 0.58 to 1.75 GHz of MeerKAT to search for both HI and OH absorbers out to $z=1.8$. The resultant dataset will provide uniquely for investigations of the evolution of the HI mass density at intermediate redshift.

Table 3 Representative Planned SKA Pathfinder Surveys

Survey	Res. [#] "	Area deg ²	z	N_{det}^{\dagger}	Ref	Note
VLA-B						
CHILES	5	0.8	<0.5	300	^a	COSMOS deep field
WSRT/APERTIF						
WNSHS*	15	3500*	<0.26	50000*	^b	Shallow, wide area
MediumDeep*	15	200*	<0.26	1×10^5 *	^c	Selected fields
ASKAP						
WALLABY	30	30000	<0.26	$> 3 \times 10^5$	^d	Shallow, wide area
DINGO-DEEP	10	150	0.1–0.26	50000	^e	GAMA region
DINGO-UDEEP	10	60	0.1–0.43	50000	^e	GAMA region
FLASH	30	targeted	0.5–1.0	few 100s	^f	HI absorption
MeerKAT						
MHONGOOSE ^{&}	12	30 x 0.8		30 ^{&}	^g	30 nearby galaxies
LADUMA	12	4	<1.4	10000	^h	ECDF-S deep field
MALS	12		<1.8	600	ⁱ	HI and OH absorbers

[#] Expected image resolution. For some surveys, the resolution may be practically limited by the heavy demands placed on computational resources.

[†] Number of predicted HI detections. In addition, stacking will also be important for many surveys.

* Survey area not yet specified, so numbers only approximate

[&] Focused on nearby galaxies but background surveyed commensally.

^a <http://chiles.astro.columbia.edu>

^b http://www.astron.nl/phisc2014/Documents/Surveys/jozsa_dwingeloo_wnshs.pdf

^c <http://www.astron.nl/phisc2014/Documents/HL.in.Galaxies/Verheijen.PHISCC2014.pdf>

^d <http://www.atnf.csiro.au/research/WALLABY>

^e <http://internal.physics.uwa.edu.au/~mmeyer/dingo/welcome.html>

^f <http://www.caastro.org/research/evolving/flash>

^g <http://mhongoose.astron.nl>

^h <http://www.ast.uct.ac.za/laduma>

ⁱ http://www.eso.org/sci/meetings/2011/gas2011/Talks/Wednesday/Gupta_chile2011.pdf

6.2.3 Exploring HI across Cosmic Time: The Next Five Years

The present review finds itself on the embarkation of several major surveys, including the full CHILES deep survey with the VLA and others planned to begin in the next few years using WSRT/APERTIF, ASKAP and MeerKAT. Table 3 summarizes some of the representative SKA pathfinder surveys as they are currently envisaged. It should be noted that the final configurations and capabilities of the pathfinders are not yet set; the parameters listed in Table 3 are current goals and may prove to be optimistic. However, all of them are likely to produce results in the next few years, taking advantages of the new capabilities now being deployed at these facilities, with first early science results already illustrating their scientific promise (e.g. Lucero et al. 2015; Hess et al. 2015; Serra et al. 2015). Of particular note, the several planned deep surveys, in combination with major efforts at other wavelengths, will allow a first exploration of the evolution of the HI mass function over the the last few billion years, laying the groundwork for the next generation of surveys exploiting the square kilometer of collecting area promised by the full SKA.

Beyond the sheer numbers of detections, important studies of the HI morphologies and kinematics for thousands of galaxies will be enabled by these future surveys. Among the pathfinders, the angular resolution of ASKAP ($\sim 30''$) and WSRT/APERTIF ($\sim 15''$) will allow WALLABY and WNSHS to obtain maps with more than 10 beams across for 800 and 300 galaxies respectively, and more than 35,000 and 10,000 galaxies will be sampled over 3-10 beams, respectively. As a follow-on to the WSRT HALOGAS survey probing to low column densities, (Heald et al. 2011), the MHON-GOOSE program will spend 200 hours per object staring at 30 nearby galaxies, delivering maps of unprecedented column density depth and probing the processes by which gas supplies are both depleted and replenished in spiral disks.

7 The Future of HI Surveys

At the time of writing of this review, plans for SKA-mid, intended to be operational in the early 2020's, suggest that some 1500 hours per year should be available for HI-related studies. A unique feature of the heterodyne techniques used in cm-wave astronomy is the potential for commensality, whereby the same acquired datastreams can be used simultaneously for both continuum and spectral line surveys (i.e., the data are acquired in spectral line mode and the continuum experiments sum the spectral channels). As has been the case for the execution of the ALFA surveys at Arecibo, there is very significant potential for commensality between future continuum and HI line surveys so that the amount of SKA-mid telescope time available for HI science may be even larger. On-going activities of the SKA Pathfinders HI Science Coordination Committee (PHISCC) revolve around coordinating the planned surveys and sharing efforts to maximize scientific productivity (Oosterloo 2015). These pathfinder surveys will only begin the exploration of the HI frontier at high redshift, allowing some quantitative input on the dominant form of gas – and even baryons – in the low mass, star forming population.

The present review has focused on the outcome and plans for surveys of the HI content of individual galaxies or of aggregates of galaxies where stacking is employed. Other compelling science is enabled by 21 cm HI line studies well beyond the limited scope of this review. Most notable among them will be: the detection of the redshifted HI line from before and during the epoch of reionization (e.g. Paciga et al. 2013; Yatawatta et al. 2013; Dillon et al. 2014; Jacobs et al. 2015); intensity mapping to probe the evolution of the baryon acoustic scale length with a single probe over a wide range of redshift (e.g., Chang et al. 2008, 2010); and using HI measures of the rotational velocity in applications of the Tully-Fisher relation to derive the local peculiar velocity field (e.g. Koda et al. 2014; Hoffman et al. 2015). For many of these and further discussions, the reader is referred to the science documents associated with the SKA science case (e.g., Carilli & Rawlings 2004, a new version of which is in the process of being updated for which many white papers are available on the arXiv). Ultimately, the construction of the full SKA will enable the detection of billions of HI galaxies throughout the universe adding a vital ingredient to our understanding of how gas has been converted into stars throughout the history of the universe.

Poised as we are on a verge of a rising wave of advanced antenna, electronic, digital, computational and algorithmic technology, the future of HI survey science will be bright indeed!

Acknowledgements We thank the entire ALFALFA survey team for their many contributions over the last decade (and more) towards observing, data processing and analysis that have led to a rich ALFALFA harvest. The ALFALFA survey team at Cornell has been supported by US NSF grants AST-0607007 and AST-1107390 to RG and MPH and by continuing support from the Brinson Foundation.

References

1. Aaronson, M., Huchra, J., Mould, J., et al., *ApJS* 50, 241 (1982)
2. Adams, E.A.K., Giovanelli, R. & Haynes, M.P., *ApJ* 768, 77 (2013)
3. Adams, E.A.K., Faerman, Y., Janesh, W.F. et al., *A&A* 573, L3 (2015)
4. Allison, J.R., Sadler, E.M., Moss, V.A. et al. 2015arXiv150307786 (2015)
5. Auld, R., Minchin, R.F., Davies, J.I. et al., *MNRAS* 371, 1617 (2006)
6. Baldry, I.K., Driver, S.P., Loveday, J. et al., *MNRAS* 421, 621 (2012)
7. Basilakos, S., Plionis, M., Kovac, K. & Voglis, N., *MNRAS* 378, 301 (2007)
8. Begum, A., Chengalur, J., Karachentsev, I. et al., *MNRAS* 386, 1667 (2008)
9. Bernstein-Cooper, E.Z., Cannon, J., Elson, E.C. et al., *AJ* 148, 35 (2014)
10. Bigiel, A., Chengalur, J., Walter, F. et al., *AJ* 136, 2846 (2008)
11. Blitz, L., Spergel, D.N., Teuben, P. J. et al., *ApJ* 514, 818 (1999)
12. Boselli, A. & Gavazzi G. *PASP*, 118, 517 (2006)
13. Boselli, A. & Gavazzi, G., *ARAA* 22, 74 (2014)
14. Bottinelli, L., Gouguenheim, L., Fouque, P. & Paturel, G., *A&AS* 82, 391 (1990)
15. Boylan-Kolchin, M., Bullock, J. S., Kaplinghat, M. *MNRAS* 415, 40 (2011)
16. Braun, R. & Burton, W.B., *A&A* 341, 437 (1999)
17. Brooks, A.M. & Zolotov, A., *ApJ* 786, 87 (2014)
18. Brown, R.L. & Roberts, M.S. *ApJ* 184, L7 (1973)
19. Cannon, J., Adams, E., Dolphin, A. et al., *ApJ* 739, L22 (2011)
20. Carilli, C. & Rawlings, S. “Science with the Square Kilometer Array: Motivation, Key Science Projects, Standards and Assumptions”, astro-ph/0409274 (2004)
21. Catinella, B. & Cortese, L. *MNRAS* 446, 3526 (2015)
22. Catinella, B., Schiminovich, D., Cortese, L., et al., *MNRAS* 436, 34 (2010)
23. Chandola, Y., Gupta, N., & Saikia, D.J., *MNRAS* 429, 2380 (2013)
24. Chang, T., Pen, U.-L., Peterson, J.B. et al., *PhysRev Lett.* 100, 091303 (2008)
25. Chang, T., Pen, U.-L., Bandura, K. & Peterson, J.B. *Nature* 466, 463 (2010)
26. Chung, A., van Gorkom, J., Kenney, J. et al., *AJ* 138, 1741 (2009)
27. Cortese, L., Catinella, B., Boisser, S. et al., *MNRAS* 415, 1797 (2011)
28. Curran, S.J., Whiting, M.T., Tanna, A. et al., *MNRAS* 429, 3402 (2013)
29. Darling, J. & Giovanelli, R. *ApJ* 572, 810 (2002)
30. Darling, J., Macdonald, E.P., Haynes, M.P. & Giovanelli, R. *ApJ* 742, 60 (2011)
31. Davies, J., Minchin, R., Sabatini, S. et al., *MNRAS* 349, 922 (2004)
32. Davies, J., Auld, R., Burns, L. et al., *MNRAS* 415, 1883 (2015)
33. Delhaize, J., Meyer, M.J., Staveley-Smith, L. et al., *MNRAS* 433, 1398 (2013)
34. Dillon, J.S., Liu, A., Williams, C.L. *Phys. Rev. D.* 89, 023002 (2014)

35. Duffy, A.R., Meyer, M.J., Staveley-Smith, L. et al., *MNRAS* 426, 3385 (2012)
36. Elmegreen, B.G., Rubio, M., Hunter, D.A. et al. *Nature* 495, 487 (2013)
37. Efstathiou, G., Ellis, R.S. & Peterson, B.A. *MNRAS* 232, 431 (1988)
38. Fabello, S. Catinella, B., Giovanelli, R. et al., *MNRAS* 411, 993 (2011)
39. Fernández, X., van Gorkom, J.H., Hess, K..M. et al., *ApJ* 770, 29 (2013)
40. Felten, J. E. *AJ* 82, 961 (1977)
41. Ferrero, I., Abbadì, M.G., Navarro, J.F. et al., *MNRAS* 425, 2817 (2012)
42. Fisher, J.R. & Tully, R.B., *ApJS* 47, 139 (1981)
43. Freudling, W., Staveley-Smith, L., Catinella, B. et al., *ApJ* 727, 40 (2011)
44. Gavazzi, G., Fumagalli, M., Cucciato, O. & Boselli, A., *A&A* 517, 73 (2010)
45. Gavazzi, G., Savorgnan, G., Fossati, M., Dotti, M., et al. *A&A* 553, 90 (2013)
46. Geha, M., Blanton, M., Yan, R, et al., *ApJ* 757, 85 (2012)
47. Genzel, R., Tacconi, L.J., Lutz, D. et al., *ApJ* 800, 20 (2015)
48. Geréb, K., Morganti, R., Oosterloo, T. et al., *A&A* 580, 43 (2015)
49. Geréb, K., Maccagni, F.M. Morganti, R. et al., *A&A* 575, 44 (2015)
50. Giovanelli, R. & Haynes, M.P. *AJ* 88, 881 (1983)
51. Giovanelli, R. & Haynes, M.P., *ARAA* 29, 499 (1991)
52. Giovanelli, R., Haynes, M.P., Kent, B.R. et al., *AJ* 130, 2598 (2005)
53. Giovanelli, R., Haynes, M.P., Kent, B.R. et al., *ApJ(Lett)* 708, L22 (2010)
54. Giovanelli, R., Haynes, M.P., Adams, E.A.K. *AJ* 146, 15 (2013)
55. Governato, F., Brook, C., Mayer, L. et al., *Nature*, 463, 203 (2010)
56. Governato, F., Zolotov, A., Pontzen, A. et al., *MNRAS* 422, 1231 (2012)
57. Grossi, M., di Serego Alighieri, S., Giovanardi, C. *A&A* 498, 407 (2009)
58. Guzzo, L., Strauss, M.A., Fisher, K.B. et al. *ApJ* 489, 37 (1997)
59. Hallenbeck, G., Papastergis, E., Huang, S., et al., *AJ* 148, 69 (2012)
60. Hallenbeck, G., Huang, S., Spekkens, K. et al., *AJ* 148, 69 (2014)
61. Haynes, M.P., Giovanelli, R. Chincarini, G. 1983, *ARAA* 22, 445 (1983)
62. Haynes, M.P. & Giovanelli, R. *AJ* 89, 758 (1984)
63. Haynes, M.P., Giovanelli, R., Chamaraux, P. et al., *AJ* 117, 2039 (1999)
64. Haynes, M.P., Giovanelli, R., Martin, A.M. et al., *AJ* 142, 170 (2011)
65. Heald, G., Józsa, G., Serra, P. et al., *A&A* 526, 118 (2011)
66. Henning, P.A., Staveley-Smith, L., Ekers, R., *AJ* 119, 2686 (2000)
67. Henning, P.A., Springob. C.M., Day, F. et al., *AIPC* 1035, 246 (2008)
68. Henning, P.A., Springob. C.M., Minchin, R. et al., *AJ* 139, 2130 (2010)
69. Hess, K.M., Jarrett, T.H., Carignan, C. et al. *MNRAS* 452, 1617 (2015)
70. Hoefl, M., Yepes, G. Gottloeber, S. et al., *MNRAS* 371, 401 (2006)
71. Hoffman, Y., Courtois, H.M. & Tully, R.B. *MNRAS*, in press (2015)
72. Hoppmann, L., Staveley-Smith, L., Freudling, W. et al. arXiv:1506.05931v1 (2015)
73. Huang, S., Haynes, M.P., Giovanelli, R. et al., *AJ* 143, 133 (2012a)
74. Huang, S., Haynes, M.P., Giovanelli, R. & Brinchmann, J., *ApJ* 756, 113 (2012b)
75. Huang, S., Haynes, M.P., Giovanelli, R. et al., *ApJ* 793, 40 (2014)
76. Hunter, D.A., Ficut-Vigas, D., Ashley, T. et al., *AJ* 144, 134 (2012)
77. Irwin, M. J., Belokurov, V., Evans, N. W., et al., *ApJ* 656, L13 (2007)
78. Jacobs, D.C., Prober, J.C., Parsons, A.R., et al., *ApJ* 801, 51 (2015)
79. Jaffeé, Y.L., Poggianti, B.M., Verheijen, M.A.W. et al., *MNRAS* 431, 211 (2013)

80. Janowiecki, S., Leisman, L., Jzsa, G. et al., *ApJ* 801, 96 (2015)
81. Jones, M.G., Papastergis, Haynes, M.P. et al., *MNRAS*, 449, 1856 (2015)
82. Jones, M.G., Haynes, M.P., Giovanelli, R. et al., *MNRAS* submitted (2015)
83. Kanekar, N. *ApJ* 797 L20 (2014)
84. Kennicutt, R.C., *Nature* 465, 559 (2010)
85. Kennicutt, R.C. & Evans, N.J. *ARAA* 50, 531 (2012)
86. Klypin, A., Kratsov, A.V., Valenzuela, O. & Prada, F., *ApJ* 522, 82 (1999)
87. Klypin, A., Karachentsev, I.m Makarov, D. et al. *MNRAS* in press (2014)
88. Kochanek, C.S. & White, M. *ApJ* 559, 531 (2001)
89. Koda, J., Blake, C., Davis, T. et al., *MNRAS* 445, 4267 (2014)
90. Kormendy, J. & Freeman, K. C., 2014arXiv1411.2170K (2014)
91. Kormendy, J. & Freeman, K. C., *Proc. of the International Astronomical Union Symposium*, 311, 77 (2015)
92. Krumholz, M.R., *Phys. Reports and astro-ph/1402.0867* (2014)
93. Krumholz, M., & McKee, C. *ApJ* 630, 250 (2005)
94. Lah, P., Pracy, M.B., Chengalur, J.N. et al., *MNRAS* 399, 1447 (2009)
95. Lang, R.H., Boyce, P.J., Kilborn, V. et al., *MNRAS* 342, 738 (2003)
96. Li, C., Kauffmann, G., Fu, J. et al., *MNRAS* 424, 1471 (2012)
97. Lucero, D.M., Carignan, C., Elson, E.C. et al. *MNRAS* 450, 3935 (2015)
98. Marinoni, C. & Hudson, M. J., *ApJ* 569, 101 (2002)
99. Martin, A.M., Papastergis, E., Giovanelli, R., et al., *ApJ* 723, 1359 (2010)
100. Martin, A.M., Giovanelli, R., Haynes, M.P. & Guzzo, L., *ApJ* 750, 38 (2012)
101. Mathewson, D.S. & Ford, V.L., *ApJS* 107, 97 (1996)
102. McGaugh, S.M., *AJ* 143, 40 (2012)
103. McConnachie, A.W., Patton, D.R., Ellison, S.L. et al. *MNRAS* 395, 255 (2009)
104. McIntyre, T.P., Henning, P.A., Minchin, R.F. et al. *arXiv:1506.07143* (2015)
105. McKee, C. & Williams, J. *ApJ* 476, 144 (1997)
106. McQuinn, K.B.W., Skillman, E.D., Cannon, J.M., et al., *ApJ* 695, 561 (2009)
107. McQuinn, K.B.W., Skillman, E.D., Berg, D., et al., *AJ* 146, 145 (2013)
108. McQuinn, K.B.W., Skillman, E.D., Dolphin, A. et al. *arXiv:1506.05495* (2015)
109. Meyer, M., Zwaan, M., Webster, R. et al., *MNRAS* 350, 1195 (2004)
110. Meyer, M.J., Zwaan, M.A., Webster, R. L. et al. , *ApJ* 654, 702 (2007)
111. Minchin, R., Disney, M.J., Parker, Q., A. *MNRAS* 355, 1303 (2004)
112. Moore, B., Ghigna, S., Governato, F. et al., *ApJ* 723, 1359 (1999)
113. Nan, R. & Li, D. *Proc. International Astron. Union* 291, 325 (2013)
114. Noterdaeme, P., Petitjean, P., Carithers, W.C. et al., *A&A* 547, 1 (2012)
115. Oosterloo, T. in “2015 PHISCC Workshop: HI Surveys Get Real”, phiscc.rutgers.edu (2015)
116. Paciga, G., Albert, J., Bandura, K. et al., *MNRAS* 433, 639 (2013)
117. Papastergis, E., Martin, A.M., Giovanelli, R. et al., *ApJ* 739, 38 (2011)
118. Papastergis, M., Cattaneo, A., Huang, S., et al., *ApJ* 759, 138 (2012)
119. Papastergis, E., Giovanelli, R., Haynes, M.P. et al., *A&A* 574, 113 (2015)
120. Peebles, J. *ApJ* 557, 495 (2001)
121. Perillat, P. *Arecibo Observatory website @naic.edu* (2015)
122. Pisano, D.J., Barnes, D.G., Gibson, B.K. et al. *ApJ* 662, 959 (2007)
123. Pontzen, A. & Governato, F. *MNRAS* 421, 3464 (2014)

124. Prochaska, J.X. & Wolfe, A.M. *ApJ* 696, 1543 (2009)
125. Rao, S. & Briggs, F. *ApJ* 419, 515 (1993)
126. Reyes, R.; Mandelbaum, R.; Gunn, J. E. et al., *MNRAS* 425, 261 (2012)
127. Rhee, J., Briggs, F.H., Lah, P. et al. (2015, in prep)
128. Rhode, K.L., Salzer, J.J., Haurberg, N.C., et al., *AJ* 145, 149 (2013)
129. Ricotti, M., *MNRAS* 392, L45 (2009)
130. Roberts, M.S. *ApJ* 161, L9 (1970)
131. Roberts, M. & Haynes, M.P., *ARAA* 32, 115 (1994)
132. Roberts, M.S., Brown, R.L., Brundage, W.D. et al., *AJ* 81, 293 (1976)
133. Rodighiero, G., Daddi, E., Baronchelli, I. et al., *ApJ* 739, L40 (2011)
134. Rosenberg, J. & Schneider, S., *ApJS* 130, 177 (2000)
135. Ryan-Weber, E.V., Begum, A., Oostelo, T. et al., *MNRAS* 384, 535 (2008)
136. Saintonge, A., Kauffmann, G., Kramer, C. et al., *MNRAS* 415, 32 (2011)
137. Salpeter, E. *AJ* 106, 1264 (1995b)
138. Salpeter, E. & Hoffman, G. *ApJ* 441, 51 (1995)
139. Sawala, T., Frenk, C.S., Fattahi, A. et al., arxiv1406.6362 (2014a)
140. Sawala, T., Frenk, C.S., Fattahi, A. et al., arxiv1412.2478 (2014b)
141. Schruha, A., Leroy, A.K., Walter, F. et al., *AJ* 142, 37 (2011)
142. Serra, P., Oosterloo, T., Morganti, R. et al., *MNRAS* 422, 1835 (2012)
143. Serra, P., Oser, L., Krajinovic, D. et al., *MNRAS* 444, 3368 (2014)
144. Serra, P., Koribalski, B., Kilborn, V. et al. *MNRAS* 452, 2690 (2015)
145. Sheth, R.K. et al., *ApJ* 594, 225 (2003)
146. Skillman, E.D., Salzer, J.J., Berg, D.A., *AJ* 146, 3 (1013)
147. Solanes, J.M., Sanchis, T., Salvador-Solé, E. *AJ* 124, 2440 (2002)
148. Springob, C.M., Haynes, M.P. & Giovanelli, R. *ApJ* 621, 215 (2005)
149. Srianand, R., Gupta, N., Momjian, E. & Vivek, M. *MNRAS* 451, 917 (2015)
150. Sterner, A., McKee, C.F., & Wolfire, M.G., *ApJS* 143, 419 (2002)
151. Suess, K., Darling, J., Haynes, M.P. et al. *AAS* 22514325 (2015)
152. Tacconi, L.J., Neri, R., Genzel, R. et al., *MNRAS* 768, 74 (2013)
153. Tanna, A., Curran, S.J., Whiting, M.T. et al., *ApJ* 772, L25 (2013)
154. Tollerud, E.J., Boylan-Kolchin, M. & Bullock, J. S., *MNRAS* 440, 3511 (2014)
155. Tolstoy, E., Hill, V. & Tosi, M., *ARAA* 47, 371 (2009)
156. Toribio, M., Solanes, J., Giovanelli, R. et al., *ApJ* 732 93 (2011)
157. Verheijen, M., van Gorkom, J.H., Szomoru, A. et al., *ApJ* 668, L9 (2007)
158. Vollmer, B., Soida, M., Chung, A. et al. *A&A* 483, 89 (2008)
159. Walter, F., Brinks, E., de Blok, E. et al *AJ* 136, 2563 (2008)
160. Wolfe, A. M., Turnshek, D.A., Smith, H.E., & Cohen, R.D. *ApJS* 61, 249 (1986)
161. Wong, T. & Blitz, L. *ApJ* 569, 157 (2002)
162. Wong, O.I., Ryan-Weber, E.V., Garcia-Appadoo, D.A. et al. *MNRAS* 371, 1855 (2006)
163. Yatawatta, S., de Bruyn, A.G., Brentjens, M.A. et al., *A&A* 550, 136 (2013)
164. Zuckerman, B. & Evans, N. *ApJ* 192, L149 (1974)
165. Zwaan, M., Briggs, F., Sprayberry, D. & Sorar, E. *ApJ* 490, 173 (1997)
166. Zwaan, M.,A., Staveley-Smith, L., Koribalski, B. et al., *AJ* 125, 2842 (2003)
167. Zwaan, M.,A., van der Hulst, J.,M. et al., *MNRAS* 364, 1467 (2005)

168. Zwaan, M., Meyer, M.J. & Staveley-Smith, L. MNRAS 403, 1969 (2010)
169. Zwaan, M.A., Meyer, M.J. & Staveley-Smith, L. MNRAS 403, 1969 (2011)